Materials Today Bio 13 (2022) 100193

Contents lists available at ScienceDirect

Materials Today Bio

journal homepage: www.journals.elsevier.com/materials-today-bio

Microfluidic mechanoporation for cellular delivery and analysis

Pulasta Chakrabarty [a], Pallavi Gupta [a], Kavitha Illath [a], Srabani Kar [b], Moeto Nagai [c], Fan-Gang Tseng [d], Tuhin Subhra Santra [a,*]

[a] Department of Engineering Design, Indian Institute of Technology Madras, Chennai, India
[b] Department of Electrical Engineering, University of Cambridge, Cambridge, CB30FA, UK
[c] Department of Mechanical Engineering, Toyohashi University of Technology, Aichi, Japan
[d] Department of Engineering and System Science, National Tsing Hua University, Hsinchu, Taiwan

ARTICLE INFO

Keywords:
Microfluidics
Mechanoporation
Cellular delivery
Transfection efficiency
Cell viability

ABSTRACT

Highly efficient intracellular delivery strategies are essential for developing therapeutic, diagnostic, biological, and various biomedical applications. The recent advancement of micro/nanotechnology has focused numerous researches towards developing microfluidic device-based strategies due to the associated high throughput delivery, cost-effectiveness, robustness, and biocompatible nature. The delivery strategies can be carrier-mediated or membrane disruption-based, where membrane disruption methods find popularity due to reduced toxicity, enhanced delivery efficiency, and cell viability. Among all of the membrane disruption techniques, the mechanoporation strategies are advantageous because of no external energy source required for membrane deformation, thereby achieving high delivery efficiencies and increased cell viability into different cell types with negligible toxicity. The past two decades have consequently seen a tremendous boost in mechanoporation-based research for intracellular delivery and cellular analysis. This article provides a brief review of the most recent developments on microfluidic-based mechanoporation strategies such as microinjection, nanoneedle arrays, cell-squeezing, and hydroporation techniques with their working principle, device fabrication, cellular delivery, and analysis. Moreover, a brief discussion of the different mechanoporation strategies integrated with other delivery methods has also been provided. Finally, the advantages, limitations, and future prospects of this technique are discussed compared to other intracellular delivery techniques.

1. Introduction

Identifying efficient delivery strategies has become necessary for a wide range of applications such as cell-based therapy, genome editing, regenerative medicine, and biological analysis [1]. Some of the significant research objectives while designing intracellular delivery platforms are ensuring high throughput, high transfections efficiency, and increased cell viability. High throughput platforms are essential to facilitate direct clinical applications as our body comprises trillions of cells, thereby requiring rapid delivery and analysis. The high throughput platforms can also provide significant statistical data, which is necessary to understand the synchronization associated with simultaneous infections for various disease analyses [2]. Healthy transfection rates and low cell deaths are indicators of a highly efficient platform. Consequently, it should be able to achieve direct cytosolic delivery of different-sized biomolecules into various cell types, including hard-to-transfect cells, with ease and simplicity [3].

Intracellular delivery strategies are popularly classified as – carrier-mediated, and membrane disruption-based methods [1,4,5]. Carrier-based techniques can be either viral [6–8] or chemical [9,10] mediated, involving endocytosis or fusion processes to internalize the targeted cargo. Although effective for gene transfer and therapy, carrier based methods are specific to cell-types, and are often restricted by cytotoxicity, and unwanted immune, inflammatory responses, leading to lower cell viabilities [4,5,8,11]. On the other hand, membrane disruption methods involve the physical penetration or permeabilization of the cellular membrane to generate transient nanopores, which then permits the delivery of exogenous molecules through diffusion or fluid convection [1,4,5,11,12]. The methods are advantageous because of minimal chances of inducing harsh cellular responses such as unwanted immunogenic or chemical reactions, thereby improving delivery efficiencies. Electroporation [13–21], optoporation [22–28], magnetoporation [29–31], acoustoporation [32–35] and mechanoporation [36–60] are some of the most popular membrane disruption techniques. Although

* Corresponding author.
E-mail addresses: tuhin@iitm.ac.in, santra.tuhin@gmail.com (T.S. Santra).

https://doi.org/10.1016/j.mtbio.2021.100193
Received 15 October 2021; Received in revised form 13 December 2021; Accepted 20 December 2021
Available online 20 December 2021

each of these methods have their own distinct features (elucidated in detail in Table 2), all of these, except mechanoporation, require an external energy field for membrane permeabilization. The mechanoporation strategies operate by imparting physical forces onto the cell membrane, which generate the transient nanopores required for biomolecular delivery. The elimination of an external carrier as well as an energy source in mechanoporation drastically reduces any chance of unwanted cell toxicity; enhancing cell viability and operational simplicity. An elaboration on these specific advantages will be the primary focus of this article.

One of the preliminary literature on mechanoporation using micropipette-based microinjection was reported in 1911 by M A. Barber [61]. While micropipette-assisted studies enable precise dosage control with high efficiency and viability, the low throughput and high operational cost restrict their usage [61,62]. These limitations were however drastically overcome with the micro/nanotechnology boom in the past few decades. With advancements in microfabrication techniques and the ability for nanoscale modulation, researchers developed an increased interest in fabricating micro/nanofluidics-based mechanoporation platforms for intracellular delivery and analysis [63–66]. Microfluidics refers to a system which deals with a small amount of fluid (10^{-9} to 10^{-18} L) through tens to hundreds of micrometers of channels [63]. These devices have very low fabrication costs, and have the advantage of being incredibly lightweight and biocompatible [12,64]. For biological studies, the miniaturization enables precise regulation over electrical, mechanical, and/or biochemical parameters, which facilitates the accurate manipulation and monitoring of cellular behavior at the single-cell level [63,64,67–71]. The potential applicability in therapeutics, diagnostics, and disease analysis has consequently stimulated a plethora of research articles on microfluidics-based mechanoporation in the last one and a half-decade.

In this review, the different microfluidic-based mechanoporation methods are broadly grouped into four categories, namely, microfluidic-based microinjection [36,37,48,54,55], micro/nanoneedle arrays [38,39,56–60], microfluidic device employing mechanical confinement [40–45], and microfluidic device employing hydrodynamic manipulation [46,47,49–53]. In a newly conceptualized section following this, we discuss about different integrated mechanoporation approaches, classifying them as hybrid mechanoporation [72–75] and mechanoporation-inspired intracellular delivery [76–80]. While the former talks about the different methods, where delivery occurs by a combination of mechanoporation with other membrane disruption-based methods [72–75], the latter incorporates key mechanoporation concepts in the device design to administer biomolecules by other intracellular delivery techniques [76–80]. An elaboration on these along with the fabrication of such devices, the materials and methods, and cellular analysis are provided. The advantages, limitations, and future prospects of these techniques are also discussed subsequently.

Although significant developments in designing microfluidic-based mechanoporation platforms have taken place, to the best of our knowledge, a dedicated review that comprehensively summarizes these different strategies is still lacking. The objective of this review, hence, is to briefly emphasize and provide an overview of different microfluidic-based mechanoporation techniques. The authors would like to mention that microinjection [62,81–84] and micro/nanoneedle arrays [85–93] are very broad fields in themselves, with a plethora of literature, which have been summarized in some detailed and dedicated reviews. The scope of this review will, however, only be to highlight some of the key developments in these areas with a focus on microfluidic-based techniques.

Table 1
Comparison between the various mechanoporation techniques.

Sl. No.	Mechanoporation Technique	Delivery parameters	Advantages	Disadvantages	Throughput (cells/min)	Transfection efficiency: Cell viability (%)	References
1.	Microfluidic-based microinjection	- Needle geometry and shape - Injection speed - Operator expertise.	- High transfection efficiency due to very accurate delivery. - High cell viability. - Uniform transfection. - Can deliver directly to the nucleus.	- Low throughput. - Expensive procedure due to the requirement of a skilled operator. - High equipment cost. - Cannot often deliver large cargo.	<100	93 : 89	[36,37,48,54,55,95,101,102]
2.	Microfluidic-based microneedle arrays	- Needle geometry, shape, density - Injection speed (for hollow injectors) - Flow parameters (for suspended cells) - Biomolecule concentration	- Larger throughput than microinjection. - High cell viability. - Localized delivery. - Simple operation procedure and ease of use.	- Complex and often expensive fabrication. - Nanoneedles often get trapped in the skin (excluding DMNs) during the removal of the device during transdermal delivery. - Show good results mostly for adhesive cells. - Non-uniform transfection.	>10,000	83 : 95	[38,39,59,60]
3.	Microfluidic device employing mechanical confinement	- Constriction geometry - Flow speed and pressure - Transit time and relaxation time - Flow parameters - No. of constrictions in series - Biomolecule concentration	- High throughput. - High transfection efficiency. - It can deliver into a large number of cell types, including hard-to-transfect cells.	- Device clogging. - Cell viability and transfection efficiency become inversely proportional after a certain range. - Show good results only for suspended cells. - Non-uniform transfection. - Cannot deliver nucleic acids.	>1,000,000	85 : 86	[40–45,150]
4.	Microfluidic device employing hydrodynamic manipulation	- Flow speed and pressure - Flow parameters - Channel geometry	- High throughput. - Delivery into a large number of cell types. - Delivery of nucleic acid with high efficiency.	- Occasional device clogging. - Non-uniform transfection.	>1,600,000	98 : 94	[47,49–53]

Table 2
Comparison between various membrane disruption-based intracellular delivery methods.

Sl. No.	Method	Delivery parameters	Advantages	Disadvantages	Throughput (cells/min)	Transfection efficiency: Cell viability (%)	References
1.	Electroporation	- Electric field parameters - Type of electrode - External environment	- High throughput. - High delivery efficiency. - Can be used for single cell analysis. - Can deliver a diverse set of biomolecules.	- Low cell viability due to the formation of irreversible pores. - Non-uniform transfection. - Requires external energy field. - Can induce toxicity.	>2,000,000	90 : 92	[5,13–21]
2.	Optoporation	- Optical field parameters - Distance between optical field and sample	- High throughput. - Contactless delivery method. - High transfection efficiency. - It can be used for single cell analysis.	- Low cell viability due to the formation of irreversible pores. - Light diffraction can often limit the performance. - Requires external energy field.	>100,000	95 : 90	[22–28]
3.	Magnetoporation	- Magnetic field parameters - Vectors to permeabilize the cell membrane	- It can be used *in vivo*. - Low toxicity.	- Low transfection efficiency. - Usability depends on the patient's age, skin structure, etc. - Requires external energy field.		40 : 75	[29–31]
4.	Acoustoporation	- Acoustic field parameters	- It can be used *in vivo*. - Low toxicity.	- Low cell viability and delivery efficiencies due to cavitation related side effects.		50 : 60	[32–35]
5.	Mechanoporation	Mentioned in detail in Table 1 for the different mechanoporation techniques	- High cell viability. - High transfection efficiency. - Requires no external energy source. - It can be used for single cell analysis. - Low toxicity.	- Device clogging is often an issue for cell squeezing and hydroporation applications. - Cell viability and transfection efficiency become inversely proportional after a specific range. - Challenging to deliver large cargo.	Mentioned in detail in Table 1 for the different mechanoporation techniques	Mentioned in detail in Table 1 for the different mechanoporation techniques	[36–45, 47–55,59, 60]

2. Microfluidic mechanoporation

In this section, the different microfluidic-based mechanoporation techniques such as microinjection, micro/nanoneedle arrays, mechanical confinement and hydroporation are discussed. All these methods demonstrate high transfection efficiency and high cell viability, with some methods demonstrating throughputs of up to a million cells per minute. A summary of key events that has led to the development of mechanoporation has been provided in Fig. 1.

2.1. Microfluidic-based microinjection

Microinjection as a method has been in existence for more than a hundred years, with one of the preliminary pieces of literature on successful delivery reported in 1911 by M. A. Barber [61]. A detailed report on the history, methodology, advantages, disadvantages, biological and instrumentation requirements, etc., for microinjection, has been provided by Shanmugam et al. [62]. In over a century of research, microinjection has been successfully delivering a variety of cargo such as organelles, peptides, DNA, RNA, antibodies, quantum dots (QDs), etc. [82] into a variety of primary and mammalian cell types [36,37,48,54, 55] as well as non-mammalian cell types [99–101]. Most of the earlier microinjection strategies were manual, performed by bringing the biomolecule-loaded nanoneedles onto the cells. For adherent cells, cell-substrate provided the necessary reaction force to facilitate injection, while micropipettes were used to hold the suspended cells during the microinjection process [62,83]. Although these methods allowed the transduction of a vast extent of biomolecules into an extensive range of single cells with good controllability, high transduction rates, and cell viability, it is limited by the requirement of a skilled technician, expensive instrumentation, and lower throughput rates [62,82,83]. Recent advances in microfluidic platform-based approaches for microinjection have reversed the microinjection strategy, incorporated automation [81] and/or robotics [84] in the process to obtain precise delivery and higher throughputs [62,82,83].

The polydimethylsiloxane (PDMS)-based microinjection strategies have been previously reported [95,101,102], but not at throughput values as reported by Adamo and Jensen [36]. A low-cost and disposable microfluidic device was employed, where cell injection took place by forcing single cells onto a stationary microneedle. The device was fabricated using SU8-based soft lithography with PDMS material. The microneedle was made of pulled glass capillaries and was precisely placed at the center of the channel by using a 3D microstage. The device comprises three microchannels, A, B, and C, as shown in Fig. 2(a). Pneumatic valves V1 and V2 regulate the fluid pressure in channels C and B, respectively. Initially, with channel B closed, cells from a supply reservoir are transported towards the biomolecule-loaded needle by the fluidic stream (Fig. 2(a)(i)). As the pressure-driven injection is

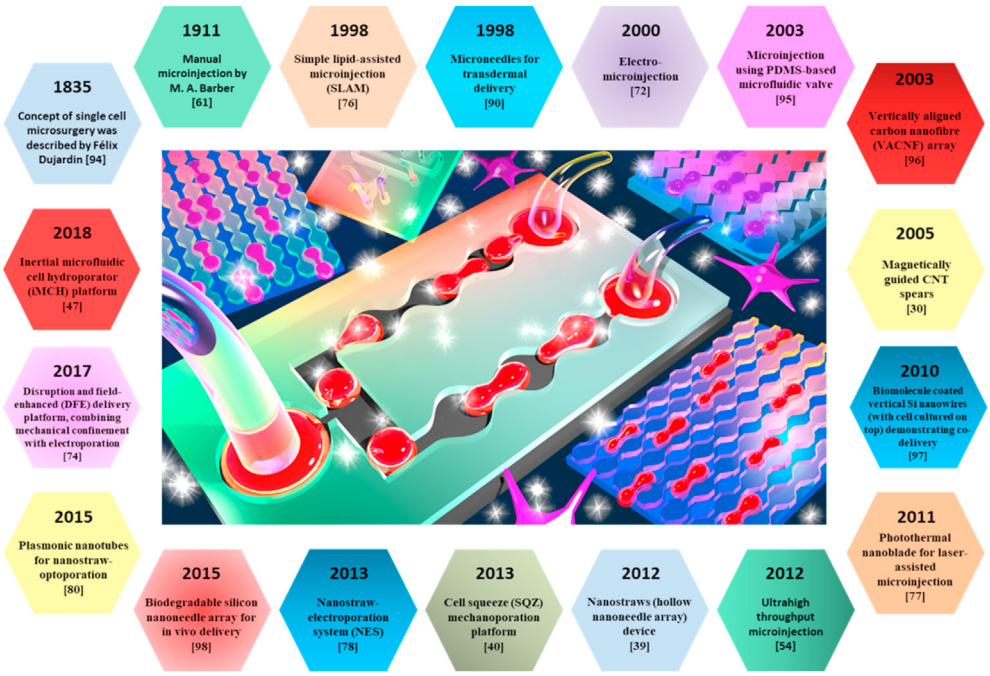

Fig. 1. Historical development of microfluidic mechanoporation

completed, the actuation of V1 closes C. It opens B, generating the back pressure required to lift the injected cell from the needle and carry it to a collection reservoir (Fig. 2(a)(ii)-(iii)). The conditions are then reversed again for the next incoming cell. The channels are designed to ensure equal pressure drops across B and C, thereby ensuring negligible changes in flow rates with valve actuation. An estimated throughput of 12 cells/hr (1 cell in 5 min) was obtained in experiments conducted with HeLa cells using fluorescently labeled dextran 10,000 Da (Da) molecules at cell flow speeds of 0.3–3 mm/s.

A cell immobilization array for microinjection was developed by Liu et al. [37,103]. As shown in Fig. 2(b)(i), an array of through-holes was patterned on a glass surface using hydrofluoric wet etching, and a PDMS-glass was bonded to the bottom surface to generate a vacuum cavity (called the PDMS spacer). As vacuum was developed in the spacer using the connection port, cells that were introduced randomly on the surface organized and immobilized themselves singularly atop each through-hole. The extra cells were removed using a transfer pipette, and the remaining cells were diagonally injected (Fig. 2(b)(ii)) using a robotic microinjection system [103] (Fig. 2(b)(iii)). The experiments using a 5 × 5 array device at low-pressure values of 1.6–2.2 kPa using mouse zygotes with phosphate-buffered saline (PBS) indicated a cell survival rate of 89.8% at a throughput of 9 cells/min. The throughput can be further enhanced with increased parallelization.

In another work, Aten et al. [48] designed a micro-electromechanical system (MEMS)-based device with a rigid-body 6-bar mechanism and a compliant parallel-guiding mechanism, which enabled a two-phase, self-reconfiguring, metamorphic motion for DNA nanoinjection. The nanoinjector fabrication was performed using polycrystalline silicon multiuser MEMS Processes (polyMUMPs), designed by MEM-SCAP Inc [104]. As shown in Fig. 3(a)(i), the nanoinjection process comprises five distinct steps. The nanoinjector, which is initially at rest, is lifted by applying a linear input force at one end of the injector mechanism. As the nanoinjector tip (lance) lifts, a positive charge is applied to it, which leads to surface accumulation of negatively charged DNA on the lance (Fig. 3(a)(ii)). The nanoinjector actuation subsequently moves the lance forward to penetrate the cell membrane, and a negative charge is then applied, which releases the accumulated DNA inside the cell in (Fig. 3(a)(iii)). The lance is then retreated out of the cell. All operations were performed with the device submerged in a PBS buffer solution. Successful DNA electro-physical transfection and gene expression was obtained using around 3000 mouse zygotes, of which about 71.9% of zygotes developed into the 2-cell stage, compared to 79.6% of untreated embryos.

Zhang et al. [54] developed a device with massively parallel injector arrays for ultrahigh throughput (UHT) microinjection. The device was fabricated using photolithography and a combination of isotropic and anisotropic dry etching on a silicon-on-insulator (SOI) substrate. As shown in Fig. 3(b)(i), negative aspiration flow generated by vertical channels called aspiration vias causes cells to draw onto an array of injectors placed inside a hemispherical capture site. The injector comprises a solid conical penetrator of sub-micron tip and a base diameter of the order of 1–2 μm (Fig. 3(b)(ii)). This provides the required minimal penetration force (and hence, minimal cell stress, maximizing reliability) as cells enter the hollow injector. Once injection takes place, positive aspiration flow releases the cells from the capture site (Fig. 3(b)(iii)), 100 × 100 array of capture sites allowed for massive parallelization. The aspiration vias were all connected to a common backside port, which led to uniform flow across each via. Cell velocity of 1 mm/s minimized membrane deformation when pierced using the micro-needle. A fully developed and steady Newtonian laminar flow through the vias was assumed. Experimental results using K-562 (human myelogenous leukemia cell line) with Propidium Iodide (PI) dye showed successful delivery. However, delivery efficiency was around 15%; the low value accounted for cell lysis due to pressure jump associated with over-population at the array during negative aspiration. An improvement to this number occurred in subsequent developments [105], which focused on optimizing the flow rate to improve the transfection efficiency and cell viability. Experiments using immortalized human T lymphocyte cell line (Jurkat) with PI dye showed ~93% transfection at a flow rate of 40 μL/min. Delivery of green fluorescent protein (GFP) plasmid in K-562 and primary human T cells occurred efficiencies of 49% and 82%, respectively, and over 87% cell viability. The device can be fabricated with over 10^7 hemispherical capture sites on a standard 4-inch Si wafer, enabling high throughput single-cell analysis.

Chow et al. [55] developed a system for high throughput automated microinjection into small adherent cells (human cells with a diameter less than 25 μm). The chip was fabricated using soft lithography technology. As shown in Fig. 4(a), the system comprises three broad sections: the

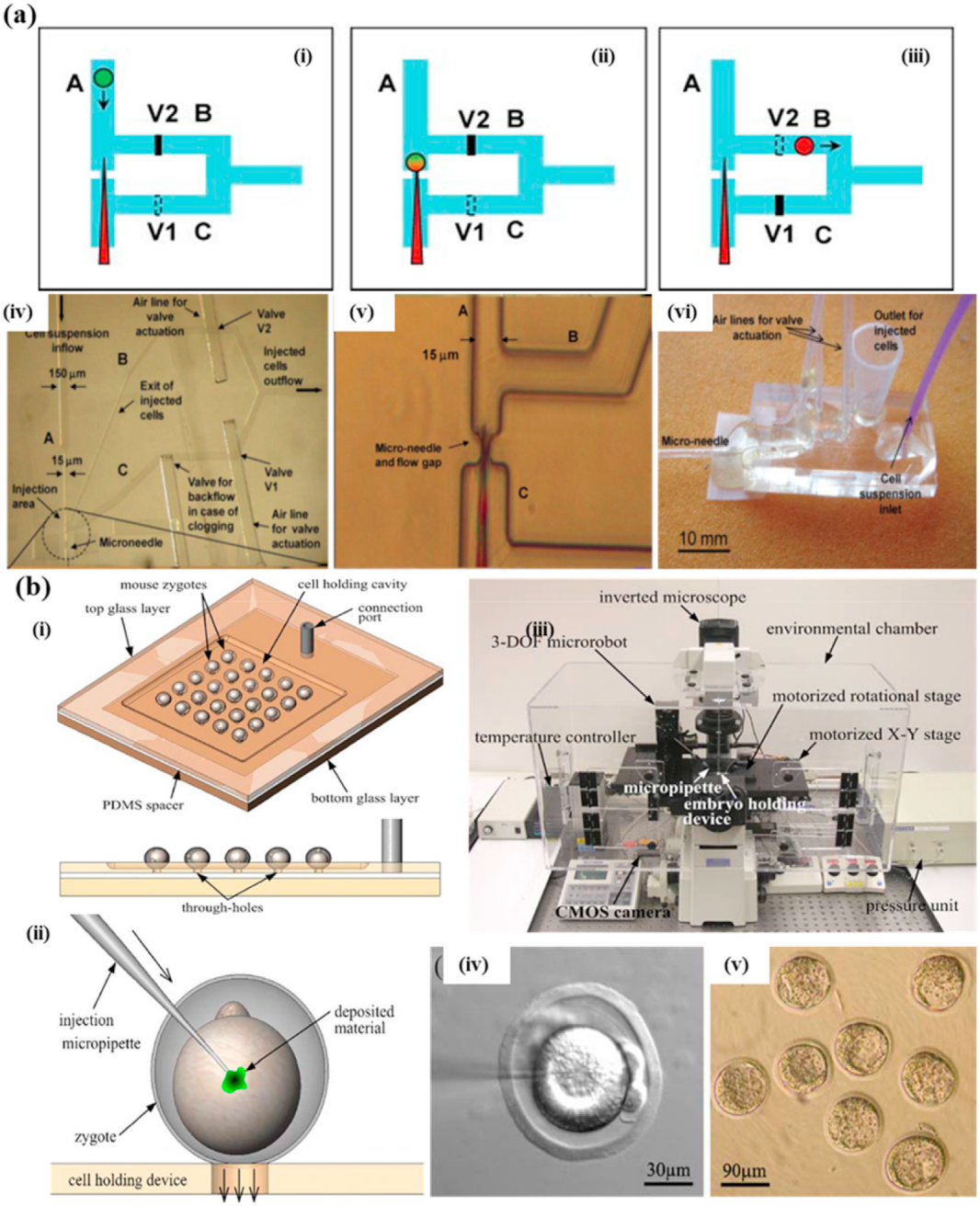

Fig. 2. (a) PDMS-based microinjection device. (i) Fluid stream moves the cell towards fixed needle (V1 open, V2 closed) (ii) Cell piercing by impinging on micro-needle. (iii) Cell lift from needle and transport to collection reservoir due to reversed fluid stream (V1 closed, V2 open). (iv) Microscopic image of the device. (v) Focused image of the nanoneedle area where microinjection takes place. (vi) Image of the final device. Reprint with permission from The Royal Society of Chemistry [36]. (b) Vacuum-based cell immobilization arrays for microinjection. (i) Schematic of the cell immobilization device. (ii) Schematic of microinjection into a single cell using the device. (iii) Schematic of the entire microinjection system. (iv) Differential interference contrast (DIC) image of micropipette injection into a mouse zygote. (v) Development of mouse zygotes into blastocysts after robotic injection. Reprint with permission from Springer [37].

injection module, the control module, and the vision module. The injection module includes the cell holder chip, micropipette, and other associated components that participate in the delivery process. The control module comprises a computer and motion controller, while the vision module comprises required cameras and light sources to identify the cell positions during the injection. The cell holder chip (Fig. 4(b)) with a bisection tree-like symmetry can trap 256 cells together in a 1-D array. A thin layer (3–5 µm) and a thick layer (10–15 µm) help provide the necessary frictional force to hold the cell during injection without compromising cell viability. The thin layer prevents cells from squeezing through the channel. The dimensions of the layers are chosen based on the diameter of the target cells such that the negative pressure traps the cells in the channel but does not allow them to pass through (Fig. 4(c)).

The injection process comprises three repeating steps – locating the position of the target cell, micropipette alignment with the target cell, and cell injection. The micropipette is kept fixed while the cell holder brings the aligned cells onto it and holds it for a certain period for injection to take place. It then goes back to its original position and shifts horizontally for the next injection to take place. This process is repeated until all cells are injected. Experiments with human foreskin fibroblast cells and human embryonic stem cell-derived vascular cardiomyocyte (hESC-VCM) using tetramethylrhodamine isothiocyanate-dextran

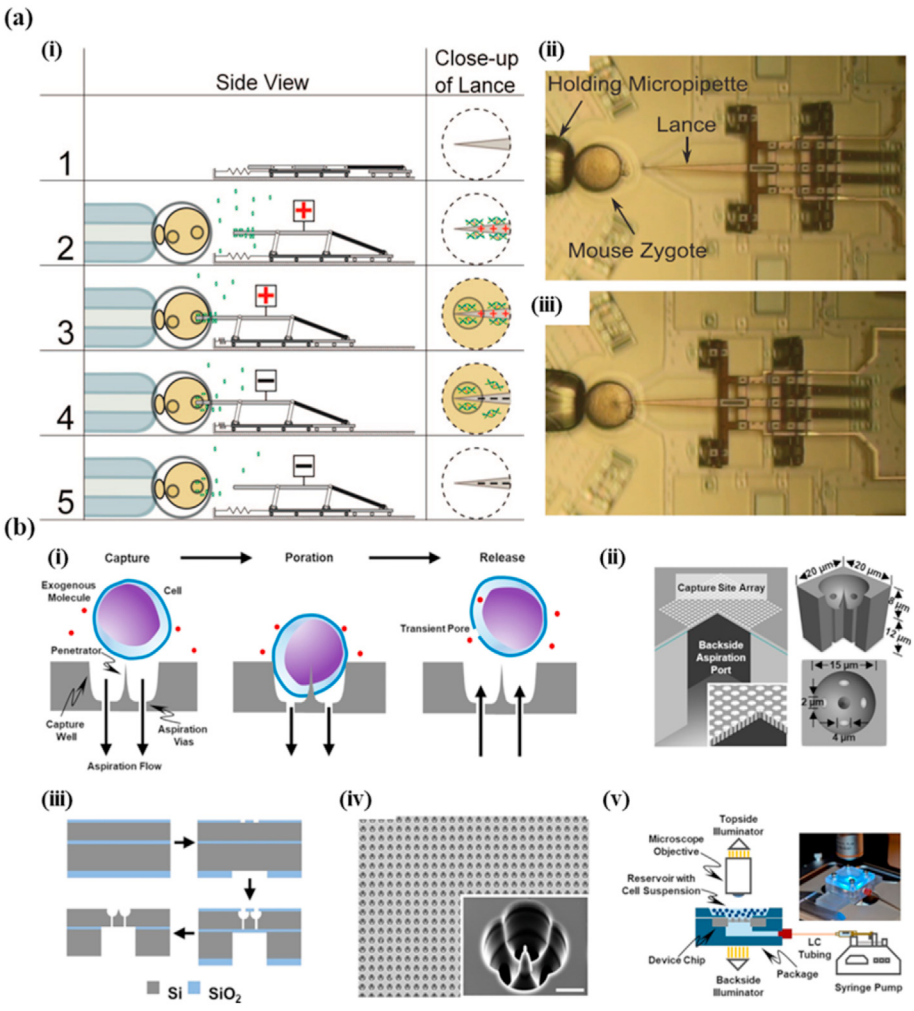

Fig. 3. (a) Metamorphic nanoinjector device. (i) DNA nanoinjection steps. Step 1: Nanoinjector at rest before any injection process. Step 2: Lance elevation and DNA accumulation on lance tip due to applied positive charge. Step 3: Cell penetration by the movement of the lance at a constant elevation. Step 4: DNA release into the cell due to applied negative charge. Step 5: Lance's movement at a constant height out of the cell. Optical microscopy image (top view) (ii) before and after (iii) nanoinjection of a mouse zygote. Reprint with permission from AIP Publishing LLC [48]. (b) UHT microinjection device. (i) Schematic of the UHT microinjection concept showing cell capture, poration, and release. (ii) Illustration of a single DMP device design (isometric view with a quarter section removed). (iii) Illustration of device fabrication on a silicon-on-insulator substrate. (iv) Scanning Electron Microscopy (SEM) image of a device portion with an inset displaying a single capture site with higher magnification (Scale bar = 5 μm). (v) Schematic of device chip packaging, placing it upon a fluorescence microscope stage and connecting it to a controllable syringe pump for manipulating the fluid in the aspiration circuit (a photograph of the final device is shown in the inset). Reprint with permission from the American Chemical Society [105].

demonstrated trapping efficiencies over 80% for both cell types. Injection efficiencies of 88.4% and 58.5% and survival rates of 63.5% and 81.5%, respectively, were obtained therein. The method could help get a throughput of 35.3 cells/min.

The above-mentioned microfluidic-based microinjection techniques develop significantly in terms of throughput when compared to conventional microinjection techniques. Although, the delivery efficiencies and cell viabilities are lower than conventional microinjection, the values are still significantly high when considering the parallelization achieved. However, the biggest drawback that comes with achieving parallel delivery is a reduction in injection uniformity. Unlike, conventional microinjection where the amount of cargo to be injected can be precisely regulated by the operator, the increase in throughput brings non-uniformity in transfection across the different cells in a sample. Also, the transfection efficiency is lower as compared to manual microinjection when transfecting larger biomolecules and DNA in various cell types.

2.2. Micro/nanoneedle arrays

Although microinjection is as an efficient tool for delivering a large number of molecules, it has very low throughput. To improve upon this, array of microneedles was fabricated, which enabled intracellular delivery with increased throughputs. In subsequent years, with advancements in micro/nanofabrication techniques, nanoneedle arrays could also be manufactured. The following section discusses the various developments in micro/nanoneedle arrays.

2.2.1. Microneedle arrays

Microneedle diameters are typically in the order of 1–300 μm, with lengths upto 1 mm. Microneedle arrays are a convenient and painless solution for transdermal delivery [85,91,106] of a wide variety of drugs [85,93,106]. For most microneedles application, as shown in Fig. 5, the device (a transdermal patch) is placed on the skin, and the needles pierce through it into the fluid stream below.

Microneedle arrays are typically divided into five different categories [85,86,89] – Hollow Microneedles (HMNs), Solid Microneedles (SMNs), Coated Microneedles (CMNs), Dissolvable Microneedles (DMNs) and Porous Microneedles (PMNs). The HMNs work on a 'poke and flow' approach (Fig. 5(a)). The biomolecule is stored in a reservoir which can be diffused to or sent at a predetermined flow rate into the skin [58, 107–109]. SMNs typically work on a 'poke, detach and diffuse' approach (Fig. 5(b)) where the poking generates transient micropores and delivery takes place by diffusion after detachment [90,110,111]. The CMNs are like SMNs, but they work on a 'coat and poke' approach (Fig. 5(c)). A layer of the biomolecule is coated and dried on the surface of the needles, which are absorbed by the flowing fluid in contact with the needle surface [112,113]. The DMNs work on a 'poke and release' approach (Fig. 5(d)). They are composed of biodegradable polymers, where the biomolecule is encapsulated in the matrix, and both dissolve over time [114,115]. The CMNs and DMNs are often grouped under SMNs because of their basic operation principle [85]. For PMNs (Fig. 5(e)), the biomolecules are pre-loaded in the microneedle and, on piercing, get released into the skin [86].

The inaugural study on microneedle arrays was performed in 1998 by

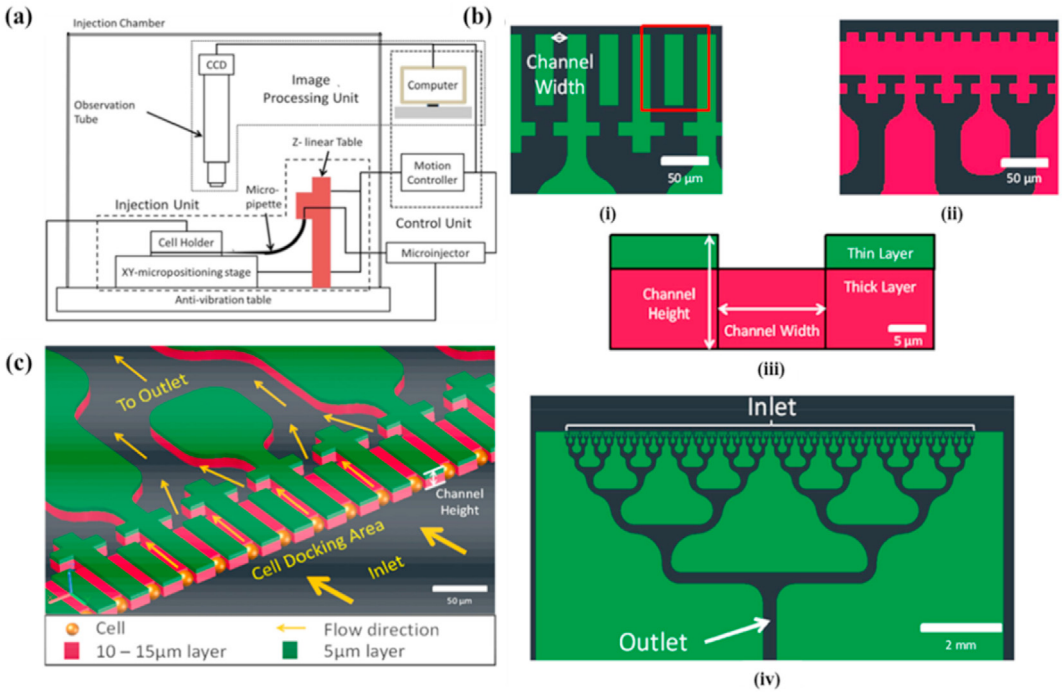

Fig. 4. High throughput automated microinjection device for small adherent cells. (a) Schematic of cell injection system with the injection module, control module, and vision module integrated. (b) Schematic of cell holder: (i) Thin layer. (ii) Thick layer. (iii) 2-layer stacked structure (front view). (iv) Overall design of the microfluidic chip. (c) 3-D view indicating flow direction when negative pressure is applied to the cell holder. Reprint with permission from IEEE [55].

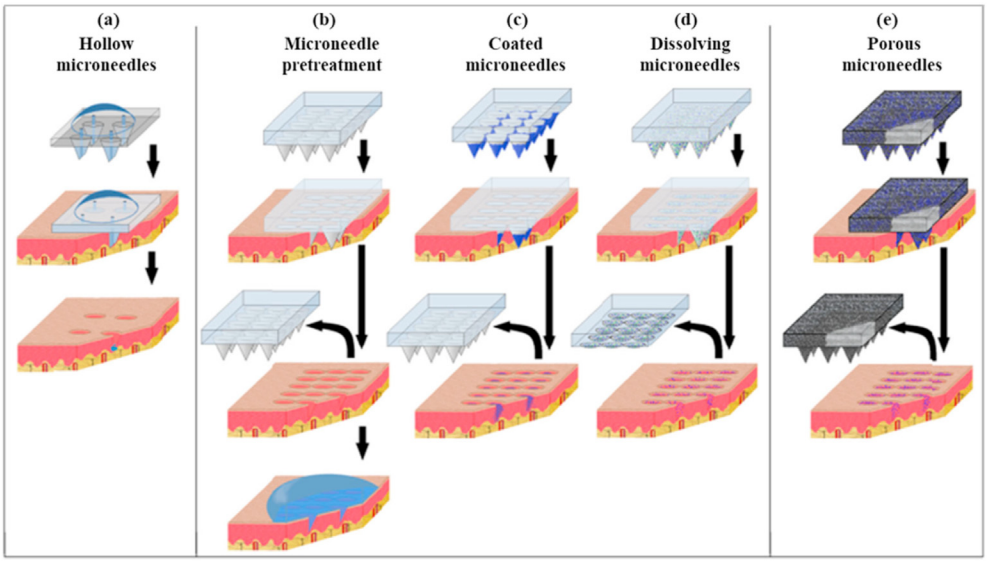

Fig. 5. Schematic of different intracellular delivery approaches using microneedle arrays. (a) Hollow microneedles. (b) Solid microneedles. (c) Coated microneedles. (d) Dissolvable microneedles. (e) Porous microneedles. Reprint with permission from Springer [86].

Henry et al. where Si microneedles, fabricated by a combination of deep reactive ion etching (DRIE) and photolithography, was used to deliver the otherwise skin-impermeable dye calcein [90]. In over two decades since then, multiple research groups have extensively worked towards developing and optimizing the microneedles geometry (length, width, density, sharpness, etc.) and shape (cylindrical, rectangular, pyramidal, arrowhead etc.) [85,93,116]. Different microfabrication techniques, such as silicon etching, photolithography, laser cutting, thin film deposition, etc., have been used to fabricate these structures [93]. Studies on fabricating microneedles with different materials (metals, polymers, ceramic, etc.) have also been performed [85,86,93,106]. Lastly, a wide range of drugs and biomolecules have been delivered using microneedle platforms, with many of these studies being FDA approved and commercially marketed [85,93,106]. The skin is also a highly beneficial location for vaccination because of its large surface area and presence of immune cells in abundance [85,91,106,117]. Apart from its ability to transdermally deliver a wide range of biomolecules, microneedle arrays have been studied for diverse applications, such as cosmetology, ocular and gastrointestinal delivery [117], glucose sensing [93,118] and transdermal fluid extraction [93,119].

There have been some notable developments in microfluidic integrated microneedle arrays [109,120,121]. For instance, Paik et al. [56]

fabricated in-plane hollow Si microneedle array, which was bonded to a PDMS microfluidic chip to perform *in vitro* and *ex vivo* delivery (Fig. 6(a)). The PDMS chip, fabricated by micromolding process, comprises of microchannels and connecting holes, which was used to inject and carry the drugs through the hollow needles, and finally into the sample. Experiments showed successful delivery of Rhodamine B dye into 1% agarose gel, chicken breast flesh and anesthetized rabbit ears. Häfeli et al. [57] designed a flexible PDMS reservoir on the back-side of a hollow Si microneedle plate. The reservoir acts as a miniature syringe, which is loaded with the target biomolecule solution, and gradually pressed using a finger to deliver them (Fig. 6(b)). Experiments using radiolabelled human serum albumin (67 kDa protein) and labeled polystyrene (PS) microspheres in mouse skin and chicken breast, respectively, demonstrated successful delivery.

Recently, Yeung et al. [58] employed a stereolithography (SLA)-based 3D-printing technique to fabricate three dimensional microfluidic device with an embedded hollow microneedle array. As shown in Fig. 6(c), the device consists of three inlets, a 3D spiral chamber and the array, which are all fabricated using a biocompatible resin. The spiral chamber was used to hydrodynamically mix the three input solution, in this case, Rhodamine B, fluorescein isothiocyanate, and methylene blue, and perform *in-situ* delivery into 2 × 2 cm porcine skin. The prescribed design was experimentally validated to be accurate, consistent and repeatable. 3D printing overcomes the equipment cost and complications associated with conventional fabrication techniques and indicates a new direction for low cost and high speed manufacturing of microfluidic microneedle platforms for transdermal delivery and biological analysis.

2.2.2. Nanoneedle arrays

Nanoneedles, like microneedles, come in various shape, size, and can be fabricated by a diverse range of materials, depending on the desired application. Their diameters are typically in the range of 10–200 nm, with a length 1–5 μm [88]. Such marginal dimensions result in minimal membrane perturbation during penetration, resulting in low cell damage. A detailed report on the historical development of nanoneedle structures has been compiled by Tay et al. [87]. While efficient for intracellular delivery, nanoneedles also find applications in diverse fields, from electrical recording to biochemical sensing [88] and immunological studies [92]. The earliest report on nanostructure-assisted delivery was obtained by McKnight et al. [96], where vertically aligned carbon nanofibres (VACNF) were used to deliver plasmid DNA, albeit with very low transfection efficiency in Chinese Hamster Ovary (CHO) cells. Similarly, Si nanowires were also studied for plasmid delivery [122]. However, the most significant results were obtained by Shalek et al. [97,123], where surface-coated Si nanowires could successfully deliver diverse molecules (DNAs, RNAs, proteins, etc.) into a wide range of cells (Fig. 7(a)). Over the past decade, extensive biological studies have been performed using Si nanowires [123–128] using a wide range of cells. Biodegradable nanoneedles were also fabricated by Chiappini et al. [98,129] for delivering nucleic acids and nanoparticles *in vivo*.

Nanostraws (nanotube or nanosyringe)-mediated delivery were initially studied by loading the target biomolecule in the nanostraw compartment with cells cultured atop them [131,132]. However, a more efficient strategy was formulated by VanDersarl et al. [39], where a microfluidic channel was integrated with the nanostraws membrane device. The nanotubes were track-etched on a polycarbonate membrane and fabricated using oxygen plasma etching, alumina deposition (using

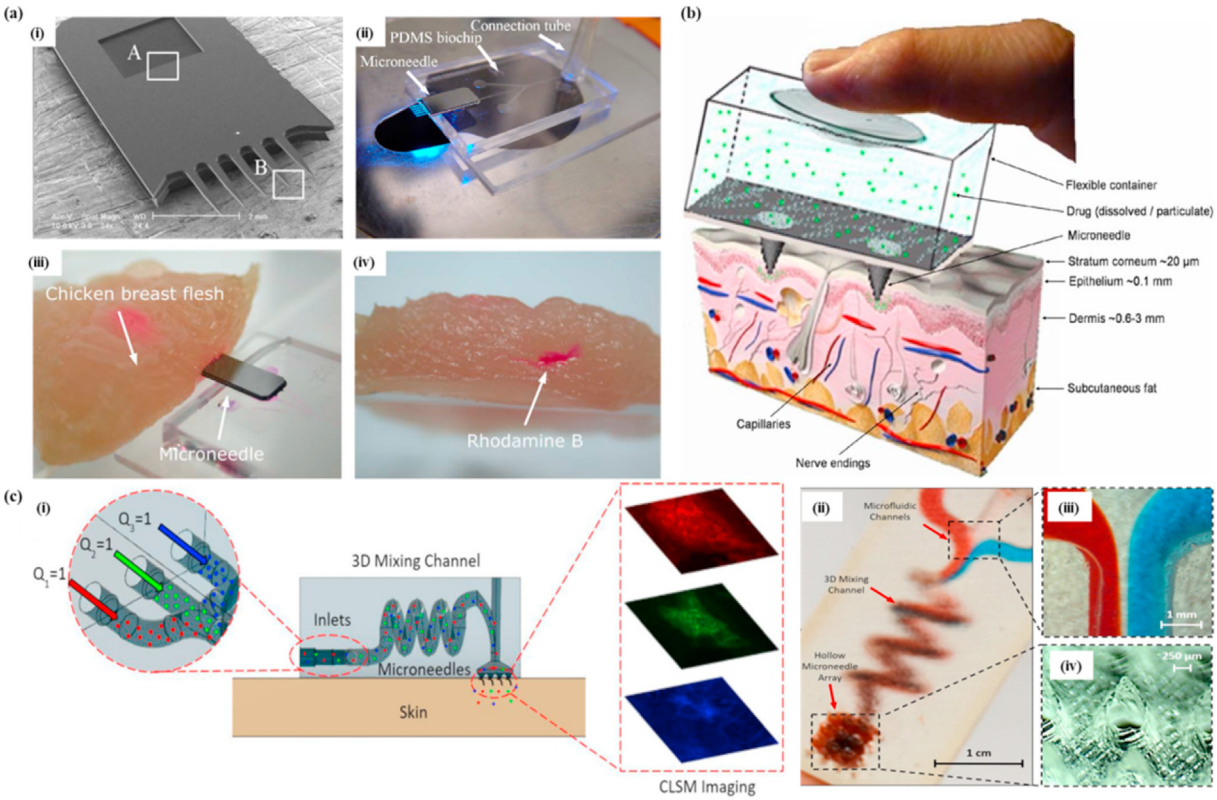

Fig. 6. (a) In-plane hollow microneedle array integrated with PDMS microfluidic chip. (i) SEM image of microneedles. (ii) Image of the microneedle array integrated with the PDMS chip. (iii) Rhodamine B injection using the device. (iv) Image showing successful injection. Reprint with permission from Elsevier [56]. (b) Schematic of hollow microneedle array with a PDMS syringe, demonstrating delivery into the skin. Reprint with permission from Springer Nature [57]. (c) SLA-based 3D-printed microneedle array device. (i) Schematic of experimental setup, showing the inlets and the 3D chamber integrated with hollow microneedle array. Inset shows the 3 inlets and confocal scanning laser microscope (CLSM) image after delivery to porcine skin. (ii) Optical image of the printed device. Inset shows zoomed in view of the (iii) inlet, showing solution mixing from the three streams, (iv) hollow microneedle array. Reprint with permission from AIP Publishing [58].

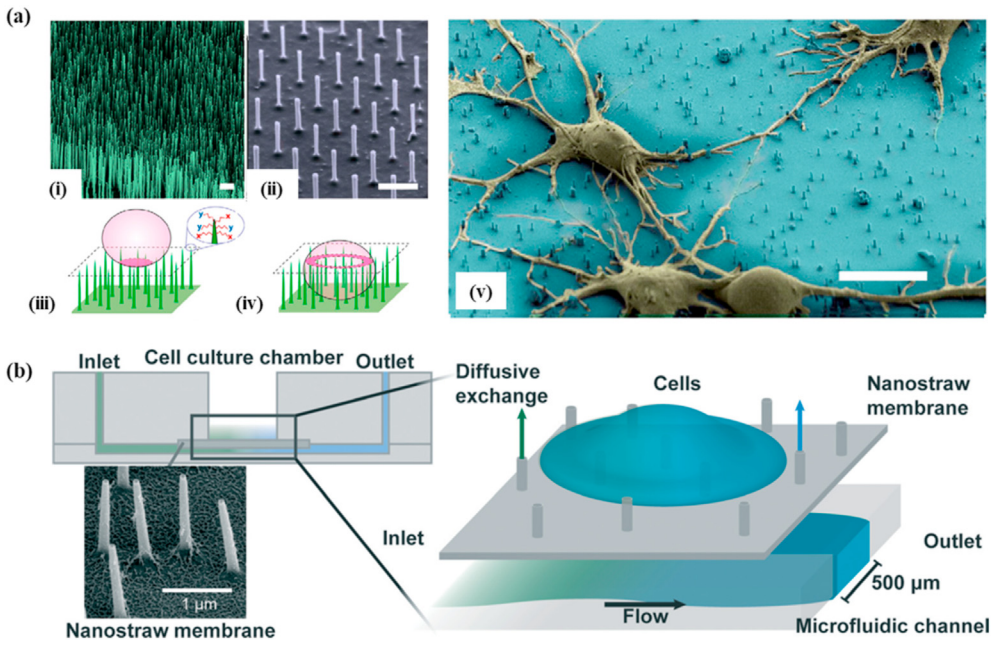

Fig. 7. (a) Vertical nanowires. (i) SEM image of nanowires fabricated by (i) chemical vapor deposition, and (ii) reactive ion etching (Scale bar = 1 μm). Schematic of a cell (iii) before, and (iv) after penetration by nanowire. (v) SEM image of rat hippocampal neurons (false colored yellow) on a Si nanowire array (false colored blue) after 1 day (Scale bar = 10 μm). Reprint with permission from PNAS [97]. (b) Schematic of nanostraws device (not drawn to scale) with microscopy image of the nanostraws. Reprint with permission from The Royal Society of Chemistry [130].

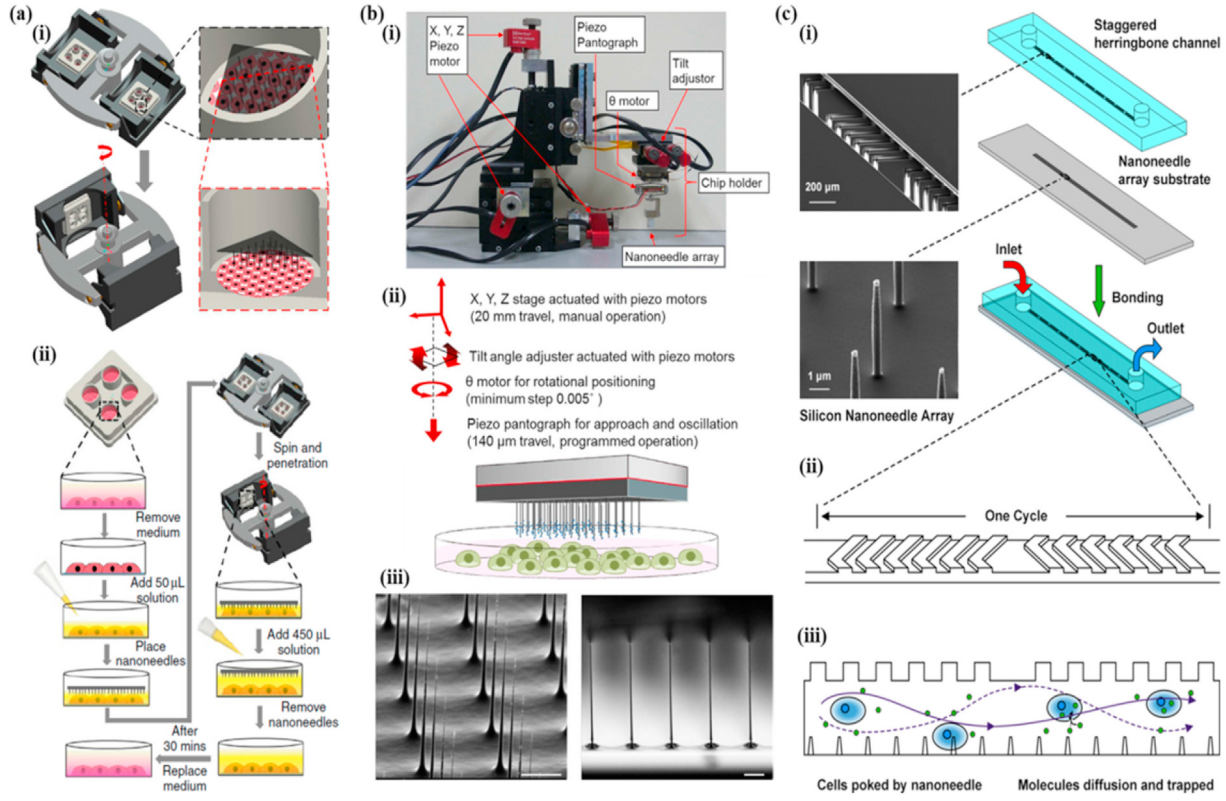

Fig. 8. (a) Solid nanoneedle array device employing centrifugation-induced supergravity. (i) Device schematic showing basic design and operating principle. (ii) Workflow of the delivery procedure using the nanoneedle array device. Reprint with permission from Macmillan Publishers Limited [59]. (b) Oscillating nanoneedle array device. (i) Picture of the nanoneedle array manipulator. (ii) Schematic representation of the different actuation methods possible using the manipulator. (iii) SEM image of nanoneedle arrays. Reprint with permission from Scientific Reports Nature [60]. (c) Solid nanoneedle array device with a staggered herringbone channel. (i) Two-layered device with staggered herringbone channel and a nanoneedle array substrate fabricated independently and then bonded together. (ii) One-cycle of the PDMS channel. (iii) Working principle of motion inside the channel and subsequent cargo delivery by nanopore generation. The asymmetric grooving induced two spinning flow lines and promoted chaotic mixing in the channel (indicated by the purple line. Reprint with permission from Bentham Science Publishers [38].

Atomic Layer Deposition), and subsequent dry etching. Control over the height, thickness, and density of the nanostraws can be easily obtained by accurately varying the different fabrication parameters [133]. A PDMS channel contained the cell culture chamber and had cells sealed above the nanostraws membrane, such that the cargo diffused through the nanostraws and delivered into the cells. The delivery of second messengers, proteins, or small molecules can occur through another PDMS channel below the nanostraws membrane, as shown in Fig. 7(b). Inlet and outlet ports were also coupled to the upper PDMS section for regulating the contents of the delivery channel. Experiments using HeLa and CHO cells indicated transfection efficiencies above 40% and 70% with GFP plasmid and Alexa-Fluor 488-hydrazide dye, respectively. Cells were viable 24 h after treatment.

A quantitative assessment of the cell-nanostraws interaction was performed to understand the effect of adhesion-promoting molecules on different parameters such as the probability and time-scale of nanostraw penetration [134,135]. Subsequent experiments to study Ca^{2+} delivery in CHO cells demonstrated cytosolic transfection in over 90% of cells within 5 s using nanostraws membranes, compared to 5% using flat membranes, demonstrating faster and efficient transfection [130]. Nearly 100% efficiency in delivering functional probes of glycosylation into CHO cells was demonstrated [136]. Successful delivery of various molecules (mRNA, siRNA, 6–2000 kDa dextran, etc.) into human hematopoietic stem and progenitor cells (HSPCs) with high transfection efficiency (up to 83%) and negligible effects on cell viability [137] was also obtained. The proposed design has been demonstrated to be a highly efficient platform for longitudinal monitoring of intracellular components in a variety of cell types [138], and it can be used as an efficient oral drug delivery device [139].

Most of the conventional nanoneedle array devices, as discussed above, demonstrate themselves as highly efficient platforms for intracellular delivery and analysis of adherent cell types. The cells are typically cultured on the nanoneedle substrate itself along with the target biomolecule. This restricts most platforms' ability to deliver biomolecules into suspended cell types. However, there are some notable exceptions. For instance, Wang et al. [59] designed a solid nanoneedle array platform, where the contact force between the nanoneedles and the cell membrane can be dynamically regulated by centrifugation-induced supergravity (Fig. 8(a)(i)). The nanodiamond nanoneedle array was fabricated by reactive ion etching on a Si substrate. As shown in Fig. 8(a)(ii), a basal medium (containing the target biomaterials) replaced the culture medium in the culture well; the volume of which was just sufficient to cover all cells and prevent them from drying up. A nanoneedle array, with the tips facing downwards (towards the cells) was gently placed on the solution, such that a thin solution layer was present between the cells and the nanoneedles. The entire setup was spun at various speeds inside a centrifuge and the optimum rpm for membrane deformation was determined. Once the centrifugation stopped, basal medium was immediately added once again to the culture well, to remove the nanoneedle array. The cells were cultured subsequently. Experiments using NIH3T3 fibroblast cells demonstrated highly efficient delivery (~60%) of 3–5 kDa dextran molecules with high cell viability (~95%) at 500 rpm. The platform also delivered of antibodies, QDs and nucleic acids (Lipofectamine 2000 complexed DNA) into primary neuronal cells with over 90% viability.

Matsumoto et al. [60] developed a nanoneedle array chip that could be oscillated using a manipulator system to perform intracellular delivery. The nanoneedles were fabricated using photolithography and a direct, reactive ion etching process on a silicon wafer. The manipulator system comprises of a piezo-actuated XYZ linear translation stage (enabling broad control over the XYZ linear motion) and a chip holder (enabling more refined control over the XY rotation, tilt angle, and movement along the z-direction) as shown in Fig. 8(b). In the chip holder, the z-direction motion was regulated by a piezo pantograph, which helped oscillate the nanoneedle array at a desired amplitude and frequency. These biomolecule-adsorbed nanoneedles repeatedly oscillated upon cells cultured on a petri dish. Intracellular delivery was demonstrated when the nanoneedles penetrated the cell membrane. Experiments conducted using nanoneedle arrays (10 μm pitch) oscillated at an amplitude of 1.0 μm, and a frequency of 5 kHz on mouse NIH3T3 cells indicated successful transfection of naked plasmid DNA and Cre recombinase with efficiencies of 34% and 42%, respectively, and with negligible effect on cell viability. Further optimization demonstrated delivery efficiency of ~45% and ~62% with 70 kDa fluorescein isothiocyanate dextran (Dex-FITC) and 3–5 kDa dextran molecules, respectively [140].

Huang et al. [38] integrated the concept of a large-scale solid nanoneedle array with a staggered herringbone channel. The patterned nanoneedle substrate was obtained through indirect microfabrication using conventional contact photolithography on a silicon substrate. The PDMS structure was spin-coated using a multilayer SU8 mold, and the two structures were bonded together using oxygen plasma. As shown in Fig. 8(c)(i), the channel of 300 μm width and 100 μm height made of periodically staggered herringbone grooves was incorporated on the top surface of a PDMS structure. The groove had a height of 45 μm, a width of 50 μm with an angle of 45° between the herringbone and the channel axis. Such a design with two asymmetrically shifted herringbone groups of six (Fig. 8(c)(ii)) promoted chaotic mixing of the channel contents coming in through the inlet port. This comprises a single cycle of motion. The vertical movement was generated due to the channel-induced chaotic flow at low Reynolds number (Re) and helped with the collision of the incoming cell on the nanoneedle substrate. This caused transient nanopores on the cell membrane and promoted biomolecular delivery through passive diffusion (Fig. 8(c)(iii)). An optimal nanoneedle dimension of 5 μm height and 400 nm diameter was chosen. Experiments using human embryonic kidney cells (HEK293A) with GFP-expressing plasmid (pEGFP-C3) indicated high gene expression efficiency (over 20%) and increased cell viability (over 95%).

To conclude, micro/nanoneedle arrays, with their simple operation procedure can deliver at higher throughputs when compared to the microfluidic-based microinjection technique with very minimal effect on cell viability. However, the method demonstrates good results, mainly for adherent cell types and only a few methods have been successful in transfecting suspended cells. The transfection uniformity is also low across the different cell types in a sample. Another major drawback when using this technique for transdermal delivery is the possibility of needles getting trapped in the skin while removing the device. Despite these, micro/nanoneedle-based platforms are highly economical, and can efficiently deliver a wide range of biomolecules without compromising on cell viability.

2.3. *Microfluidic device employing mechanical confinement*

To overcome the limitations of micro/nanoneedle arrays for high throughput transfection of suspended cells, many researchers have designed microfluidic platforms to permeabilize the membrane by passing cells through physical constrictions. The dimension of these constrictions are less than that of the cell, resulting in squeezing. A detailed review of the theoretical aspects of cells passing through constrictions and undergoing squeezing has been provided by Zhang et al. [141]. An in-depth understanding of cell migration through micro-constrictions can provide a comprehensive understanding of many medical issues such as cancer metastasis and embryonic development [142].

The primary parameters that govern cell squeezing and delivery are the transit time across the confinement, the pressure at which the cell-biomolecule mixture is flowing, flow velocity, and non-dimensional parameters (such as Reynolds Number, Bond Number, Weber Number, etc.) [141]. The travel time also depends significantly on cell diameter and cell stiffness [143]. The width (diameter), length, number of microfluidic constriction channels in series, and biomolecule concentration are also important delivery parameters. Since most of the delivery process is diffusion-dominated, a greater concentration of the deliverable

biomolecules or materials is preferred to achieve high efficiency. The diffusivity and diameter of the target biomaterial are also essential parameters [144].

One of the most innovative works was performed by Sharei et al. [40], where multiple cells underwent mechanical deformation simultaneously when passed through parallel micro constrictions channels. This has been referred to as an SQZ platform. The channels were fabricated on a silicon wafer using photolithography and a direct reactive ion etching process, with a pyrex layer used to seal it. The system was mounted on an interface made using stainless steel and aluminum, connected to the chip using inert O rings. As shown in Fig. 9(a), transient disruptions of cellular membrane occurred when cells were passed through a constriction channel smaller than the cell diameter. This facilitated the passive diffusion of materials into the cytosol. The device consisted of 45 parallel microfluidic channels, which were identical and contained parallel constrictions, 4–8 μm in width and 10–40 μm in length. This helped study the effect of varying the constriction geometry for analyzing delivery efficiency and cell viability. The parallel channels prevented device failure due to clogging in any one channel, thereby ensuring uniform cell treatment and high throughput at the single-cell level. A pressure regulator was used to drive the mixture of cells and deliverable biomolecules with constant pressure from an inlet reservoir and through the device, with the treated cells being collected at the reservoir outlet.

Experiments conducted using fluorescently labeled 3-kDa and 70-kDa dextran on a wide range of cell types such as human foreskin fibroblasts (NuFFs), primary murine dendritic cells, and embryonic stem cells showed successful transfection after undergoing squeezing through the device (Fig. 9(b)(i)-(iii)). Flow cytometry indicated 70–90% cytosolic delivery efficiency within the first minute of treatment. Increasing constriction length and decreasing constriction width significantly enhanced delivery efficiency for all operating speeds. A greater number of constrictions in series also improved the efficiency. However, an increase in delivery efficiency was accompanied by a decrease in cell viability. The design provided a throughput of 20,000 cells/s before failure took place by device clogging.

Subsequent experiments focused on studying the efficacy of this platform to deliver different types of materials into various cell types. Successful cytosolic delivery of carbon nanotubes (CNTs) (Fig. 9(b)(iv)), gold nanoparticles (AuNPs), antibodies [40], and QDs [145] were demonstrated using HeLa cells. Simultaneous delivery of a diverse set of biological macromolecules (such as polysaccharides, nucleic acids, etc.) and antigen into human and murine immune cells (such as T cells, B cells, etc.) was demonstrated [146–148]. Studies on understanding the recovery kinetics of the cell membrane post deformation indicated that calcium content of the exogenous buffer, ambient temperature condition, and increased cell incubation time after treatment enhanced surrounding biomolecular uptake [149]. Delivery could also be significantly optimized by using specific constriction widths for particular cell types [150]. The platform was also successful in high throughput protein labeling [151].

In another study, Liu et al. [41] designed performed a comprehensive analysis of the volume exchange by cells during squeezing (Fig. 10(a)). Mathematical modeling of the cell volume exchange for convective transfection (cell VECT) before and during compression was examined. Combined with experimental results, the authors concluded that when cells are subjected to compressive forces, cytoplasmic expulsion occurs. However, after removing the forces, the cells recovered to their original size and shape by absorbing extracellular fluid from the surrounding medium. Further results indicated that when cells are subjected to squeezing through multiple constrictions, increasing the relaxation time between two consecutive squeeze-passes enhances the volume uptake and cargo delivery. The integrity of the nuclear envelope is maintained during compression and cells undergo minimal protein loss after the volume exchange [152]. The platform was also demonstrated as an efficient tool for labeling autologous therapeutic cells [153]. Recently, using VECT, successful mRNA transfection in a variety of primary human cells (such as T cells, HSPCs, natural killer cells) was demonstrated with a maximum transfection efficiency of 80% [154]. Such high delivery efficiency values at such lower amounts of mRNA payload have not been yet been demonstrated by the currently available mechanoporation platforms.

Han et al. [42] analyzed the delivery efficiency and cell viability by optimizing the physical constrictions of the microfluidic device. The device fabricated using PDMS on a silicon wafer was employed with 14 identical scattering and deformable zones, with each zone containing ten microconstriction rows. As shown in Fig. 10(b)(i), the microfluidic platform was designed with differently-shaped constrictions, each varying in dimension and shape. Cell passes through the deformation zone of the micro-constrictions channel, generating transient holes for biomolecular delivery through the passive diffusion process (Fig. 10(b)(ii)). The

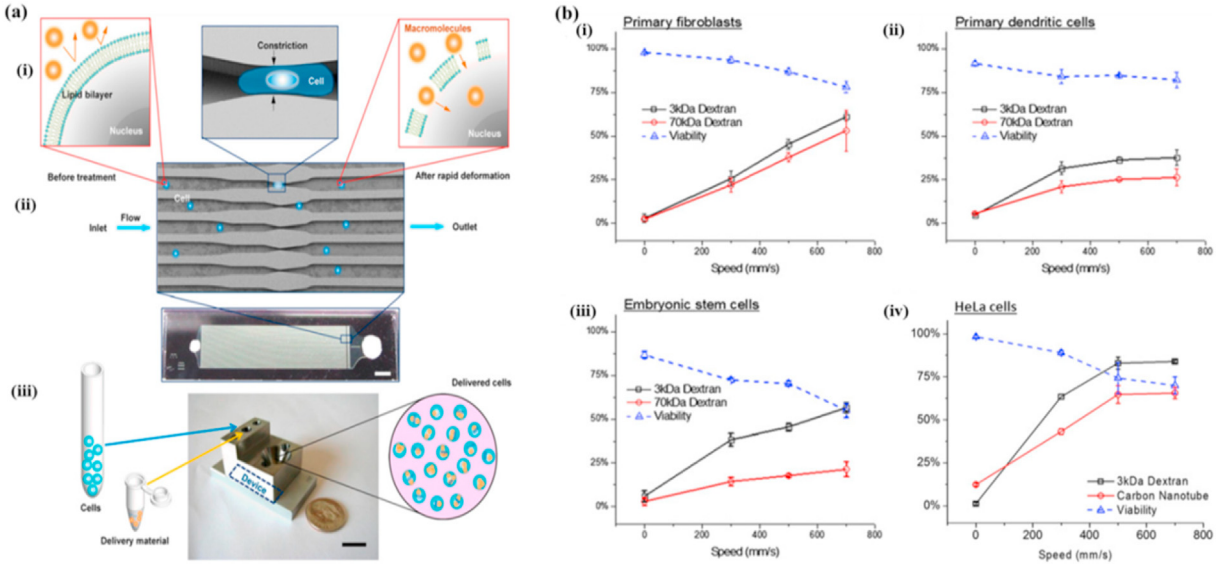

Fig. 9. Cell squeezing (SQZ) device. (a) (i) Illustration of device methodology for transient cell membrane disruption when passed through micro constrictions. (ii) Zoomed-in image of the finished device showing parallel constrictions. (iii) Image explaining delivery procedure from inlet to outlet reservoir through the chip. (b) Delivery efficiency and cell viability of (i) NuFFs, (ii) primary murine dendritic cells (iii) embryonic stem cells, demonstrating 3-kDa and 70-kDa dextran delivery, measured by flow cytometry. (iv) Delivery efficiency and cell viability of Hela cells demonstrating 3-kDa and CNT delivery. Reprint with permission from PNAS [40].

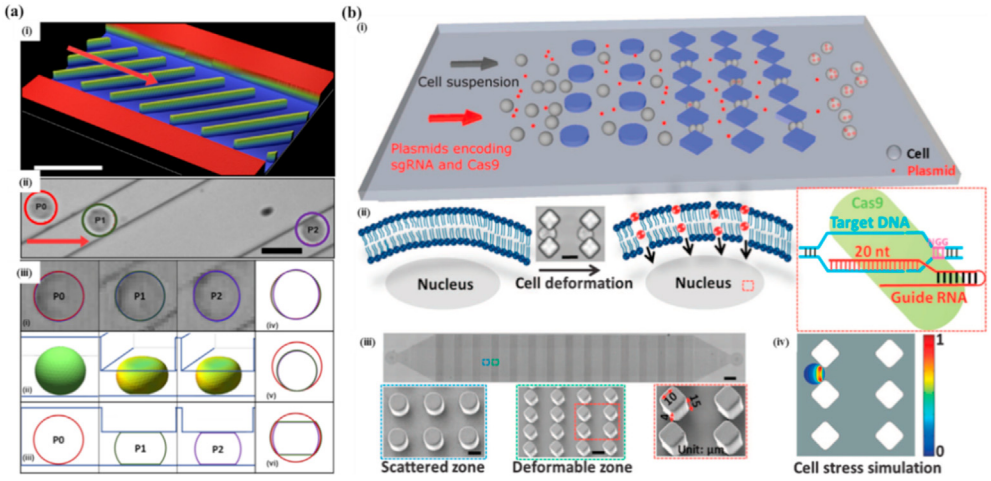

Fig. 10. Cell squeezing devices. (a) Illustration of cell flow and compression. (i) Microfluidic device with diagonal ridges. The red arrow indicates the direction of cell flow. (ii) A single cell at multiple positions (P1, P2, and P3), passing through the channel. (iii) (i) Top view corresponding to P1, P2, and P3. (ii) 3-D representation of cell flow before entering the ridge (P1) and during compression in the ridge (P2, P3). (iii) Side view corresponding to P1, P2, and P3. (iv) Top view. (v) Spherical projection of the cell. (vi) Side view. Reprint with permission from Elsevier [41]. (b) (i) Deformation of cells when passed through microconstrictions. (ii) Illustration of cell deformation, transient hole generation, when passed through microconstrictions, and genome editing (Scale bar = 15 mm). (iii) Microscope image of the device (Scale bar = 0.5 mm), SEM image of the scattered and deformable zones (Scale bar = 15 mm), Image of single microconstriction of 15 mm in depth, 4 mm width, 10 mm length. (iv) Cell stress simulation when passing through a microconstriction and subsequent stress gradient on cell. Reprint with permission from the American Association for the Advancement of Science [42].

scattering zone scatters the cell suspension and prevents device collapse (Fig. 10(b)(iii)). The constriction dimensions were optimized through subsequent experiments, and the diamond pattern demonstrated optimum results. Experimental results showed successful transfection of plasmids encoding sgRNAs and Cas9 into various cell types. The authors concluded that the proposed system could be an efficient tool for the high throughput delivery of CRISPR-Cas9 into the cell.

Modaresi et al. [43] designed a microfluidic platform, where the cells

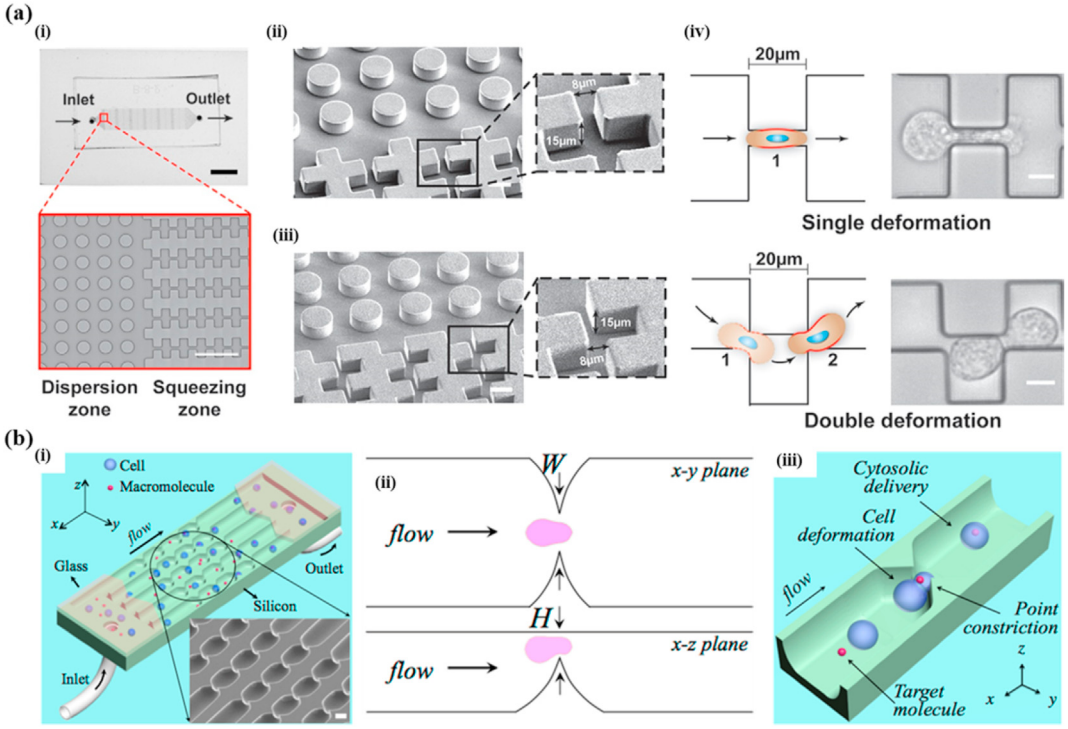

Fig. 11. Cell squeezing devices. (a) Cell squeezing using double deformation device. (i) Microscope image of the device (Scale bar = 100 μm) with a zoomed view (Scale bar = 5 mm). (ii) SEM image of single deformation device (Scale bar = 20 μm). (iii) SEM image of double deformation device (Scale bar = 20 μm). (iv) Schematic and bright field imaging of cell squeezing for the two processes. Reprint with permission from WILEY-VCH Verlag GmbH & Co [43]. (b) Cell squeezing using 2-D point constrictions. (i) Illustration of intracellular delivery using the microfluidic platform. The inset is a micrograph showing a zoomed-in section of the device without the cover glass (Scale bar = 20 μm). (ii) Illustration of a single cell passing through the constrictions and undergoing deformation in two dimensions. (iii) 3-D illustration of cell deformation and delivery when passing through the channel. Reprint with permission from the American Chemical Society [44].

underwent double deformation. Fig. 11(a)(i) shows the proposed method, where two microfluidic devices are developed - one which allows only a single deformation (Fig. 11(a)(ii)) and the other enabling double deformation (Fig. 11(a)(iii)). Device fabrication was performed using SU-8-based soft lithography with PDMS material. These chips have seven dispersion and twelve squeezing zones. The pillars of the dispersion zone for both designs contain PDMS pillars of 20 μm in diameter and 15 μm in height, separated from each other by a distance of 30 μm. For the squeezing zones, the first design was performed by orienting the 20 μm constrictions to form tunnels and enabling single deformation (Fig. 11(a)(iv) top). In contrast, the orientation for the second device was evolved to form squeeze constrictions (Fig. 11(a)(iv) bottom). The gap between the microconstrictions was chosen to be 8 μm. Experimental results on human-adipose-derived stem cells (hASCs) with Dex-FITC indicated that double deformation demonstrated higher internalization of the materials into cells than the single deformation. The device is very suitable for delivering small size biomolecules. The proposed method showed high delivery efficiency (~85%) and increased cell viability (>80%) with higher throughput than the single deformation method without inducing cell apoptosis.

Xing et al. [44] reported the effect of intracellular delivery when cells are squeezed using point constrictions in two dimensions instead of one-dimensional squeezing as in the cases discussed above. The design comprised an array of microchannels, each of which contained multiple single-cell constrictions in series (Fig. 11(b)(i)). The channels were fabricated on a silicon wafer using photolithography, advanced oxide etching, and a direct reactive ion etching process, with a pyrex layer used to seal it. The values of maximum constriction width (W) and maximum constriction height (H) were chosen in such a way that the channel dimension was lower than the diameter of the passing cell (Fig. 11(b)(ii)). This led to cell squeezing and subsequent cytosolic delivery, as shown in Fig. 11(b)(iii). Experiments using human colorectal carcinoma cells (HCT116) with fluorescein-conjugated 70 kDa dextran flowing at 4 bar pressure demonstrated high delivery efficiency (~86%) and increased cell viability (~85%). The proposed method required less backpressure than a single rectangular constriction due to minimal interaction with the surface, subsequently requiring lower flow rates. The device achieved a high throughput of 2500 cells/s.

In a very recent work, Hao et al. [45] designed a nanofluidic device, which promoted high throughput delivery of exogenous cargos into exosomes. The device, named an exosome nanoporator (ENP), comprises of 21 microfluidic channels (10 inlet channels and 11 outlet channels) aligned in parallel and 1500 nanochannels interlinking a pair of inlet and outlet channels (equating to 30,000 nanochannels on the ENP device), as shown in Fig. 12(a). The microchannels were fabricated on a PDMS layer using soft lithography, which was then plasma bonded onto the perpendicular nanochannels, fabricated by reactive ion etching on a glass substrate. As shown in Fig. 12(b), the exosomes and cargo molecules enter the device through the inlet channel and are guided to the nanochannels by the fluid flow. A nanochannel depth of 130 nm (comparable to exosome dimensions) helped generate transient nanopores on the exosome membrane by a combination of mechanical compression and fluid shear. The cargo from the surrounding medium is then convectively delivered into the exosomes and the transfected exosomes are collected at the outlet. Experiments using exosomes purified from human non-small cell (A549 lung cancer cells) using Alexa Fluor 488-labeled 3 kDa and 10 kDa dextran molecules demonstrated loading efficiency of 37% and 31%, respectively. While most of the literatures discussed in this article focus primarily on intracellular delivery, the study of high throughput intra exosomal delivery opens new pathways for the use of exosomes as smart drug-carrying vehicles that can be used for cellular research and biological analysis.

Mechanical confinement is highly advantageous because of its ability to perform high throughput delivery of a large variety of micro and macromolecules into a large number of cells. These devices have a simple layout, are easy to fabricate and the operational steps are very convenient. These advantages enable researchers to use the mechanical confinement devices to perform single cell analysis at throughput values way greater than the methods previously discussed. However, despite their ability to perform cytosolic delivery of small-sized molecules with high transfection efficiency, the values reduce when nuclear penetration is desired or when the target biomolecule size increases. The process is also highly stochastic, which leads to uneven delivery. Although, the designs have been highly successful in transfecting suspended cell types, they have not yet been demonstrated for adherent cells. Another major limiting factor of these design is the clogging issue, which renders the device useless after a couple of runs.

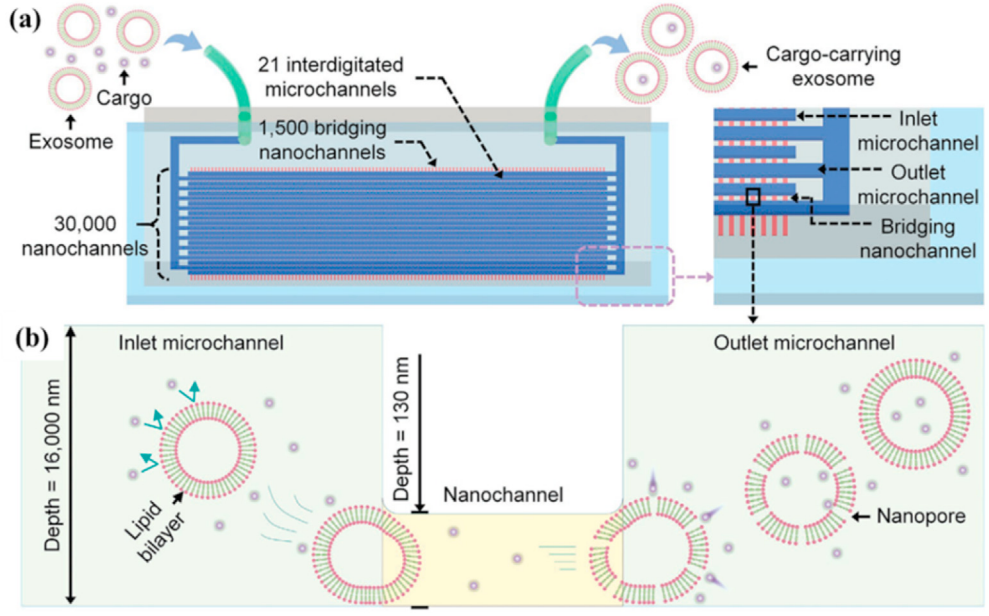

Fig. 12. Exosome nanoporator (ENP) device. (a) Schematic of the ENP device. (b) Working principle of the device demonstrating cargo loading into exosomes after being subjected to mechanical compression and fluid shear in the nanochannel. The channel dimensions are represented. Reprint with permission from WILEY-VCH Verlag GmbH & Co [45].

2.4. Microfluidic device employing hydrodynamic manipulation

Devices employing cell squeezing methodologies, as discussed in Section 2.3, have achieved high throughput, but their performance is often limited by channel failure due to device clogging. To overcome this, many research groups have designed microfluidic devices, where hydrodynamic forces were used to regulate the cell-fluid flow. This method is referred to as hydroporation. Single cells were poked, and in certain cases, stretched or squeezed (or both) in a microchannel, leading to transient pore generation and material delivery by a combination of diffusion and/or fluid convection. As the cells were not being squeezed using constriction channels, the chance of device clogging and cell lysis is minimal. Hydroporation techniques are advantageous because of the simplicity in their design, the requirement of inexpensive equipment, and, as will be seen subsequently, their ability to demonstrate high throughput delivery of different biomolecules into a wide variety of cells.

A microfluidic chip was designed by Adamo et al. [46], where intracellular delivery into suspended cells was performed by firing a high-speed liquid jet. As shown in Fig. 13(a), the device comprises of a channel through which the cells flow, a nozzle at the top this channel and a fluid chamber containing the target biomolecule, and. Fabrication was performed by a combination of photolithography and DRIE. As cells flowed pass the micron-sized nozzle, pressure pulses was applied to the chamber by compressing a piezoelectric membrane. This ejected a small volume of the target biomolecule with sufficient energy to penetrate and deliver into the cell. Cell alignment in front of the nozzle was performed by visual inspection. Experiments using fluorescently labeled 10 kDa dextran with HeLa cells indicated successful delivery using this method.

Deng et al. [47] reported an inertial cell flow in the channel, causing cells to collide at a T-junction and form transient membrane pores, facilitating biomolecular delivery through passive diffusion. The chip was fabricated using soft lithography technology. As shown in Fig. 13(b)(i), the design comprises three systematic steps. In step (i), cells and the target material are injected into the channel using a syringe pump. In step (ii), the inertia of the fluid positions the (previously) randomly aligned cells at the center of the channel. Finally, in step (iii), the flowing cells collide at the channel wall at the T-junction containing a sharp tip. This cell-wall collision coupled with the fluid-shear induced sufficient membrane disruption to generate transient nanopores for biomolecular delivery through the passive diffusion process. The presence of a tip ensures an effective stress concentration required for efficient delivery. The cell-wall collision image using a high-speed microscope is shown in Fig. 13(b)(ii). The system was operated at moderate Re of 1–100, which allowed for accurate cell positioning at the center of the channel (over 99% focusing efficiency) by utilizing the inertial effects of fluid flow. Experiments using Dex-FITC in the MDA-MB-231 cell line demonstrated high delivery efficiency (>80%) and cell viability (>80%) at Re 325. Delivery efficiency increased, and cell viability decreased with increasing Re. Further studies indicated that different biomolecules such as plasmid DNA, CRISPR-Cas9, and DNA nanostructures were effectively delivered using this device. A throughput of 1,000,000 cells/min was achieved with a single channel. In a subsequent development [49], the sharp tip was replaced with a cavity, causing cells to collide with a fluid wall and not a PDMS tip. This resulted in lesser cell perturbation, increased cell integrity and fewer chances of clogging. The design consequently demonstrated higher transfection efficiency (~98%) and cell viability (~90%) than the previous design.

Another non-collision-based approach developed by Kizer et al. [50] eradicated any chance of partial clogging as with the previous designs. The design worked on the same operating principles for cell-nanomaterial injection and alignment as demonstrated by the earlier devices and was also fabricated similarly [47,49]. However, in the proposed system, transient cell membrane pore formation took place by rapid hydrodynamic shearing of the cells (Fig. 14(a)). As cells reached the cross-section, they underwent hydrodynamic stretching, consequently forming transient pores. In addition to diffusion-based delivery, as discussed in most literature, this method also led to a convection-based delivery due to the rapid solution exchange across the cell membrane during the squeezing process. Flow rates could be adjusted to vary the transfection efficiency. The efficiency increased, and cell viability decreased with increasing Re. Experimental results demonstrated effective delivery of DNA origami nanostructures into a variety of cell types (K-562, MDA-MB-231, HeLa cells, etc.) with high efficiency (up to 90%), increased cell viability (~80%) and high throughput (>1,600,000 cells per min).

In a very innovative study, Joo et al. [53] designed a droplet mechanoporation device, where membrane permeabilization occurs by allowing cell-biomolecule encapsulated droplets to squeeze through multiple constrictions. As shown in Fig. 14(b)(i)-(ii), the platform consists of two distinct units – a droplet generator followed by a cell membrane perforator. The oil was injected through two inlet channels separately and a flow-focusing droplet generation scheme [155] was employed to create the cell-biomolecule encapsulated droplets. The channels were fabricated by PDMS-based soft lithography. The authors hypothesized that as the droplets squeezed through the constrictions, internalization of biomolecules through the permeabilized membrane occurred by a combination of convection and diffusion-mediated transport. Since, the required cargo is loaded into each individual droplet and the microchannel is mostly occupied by the carrier oil, far lower quantity of cargo is utilized with negligible clogging. Experiments using a variety of immune cells with different genetic molecule (<2000 kDa dextran, 996 nt mRNA, 7.9 kbp plasmid DNA), showed maximum transfection efficiency of ~98% at very high throughputs (10^6 cells/min).

Kang et al. [51] generated a spiral vortex flow (Fig. 15(a)(i)), and cells within this flow regime were subjected to hydrodynamic deformation. The technique, as shown in Fig. 15(a)(ii), was named spiral

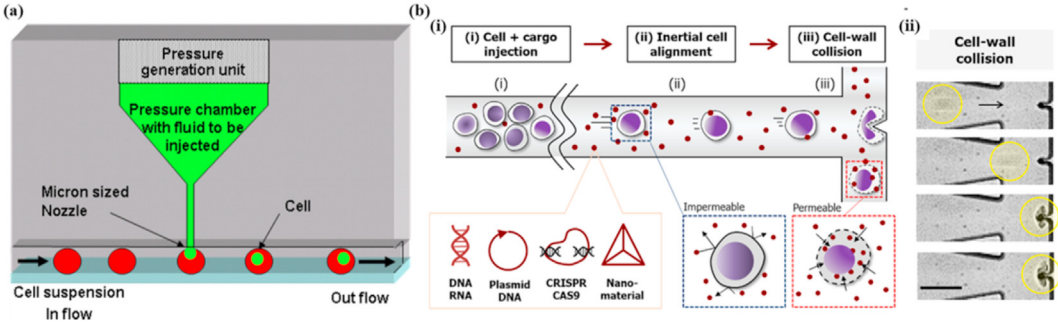

Fig. 13. (a) Schematic of microfluidic jet injection. Reprint with permission from IOP Publishing Ltd [46]. (b) Inertial microfluidic cell hydroporator (iMCH). (i) Schematic of the working mechanism of the proposed device. The device is capable of delivering a wide range of materials into the cell. (ii) Cells colliding onto a sharp tip at the T-junction present on the channel wall were captured using a high-speed microscope. Reprint with permission from the American Chemical Society [47].

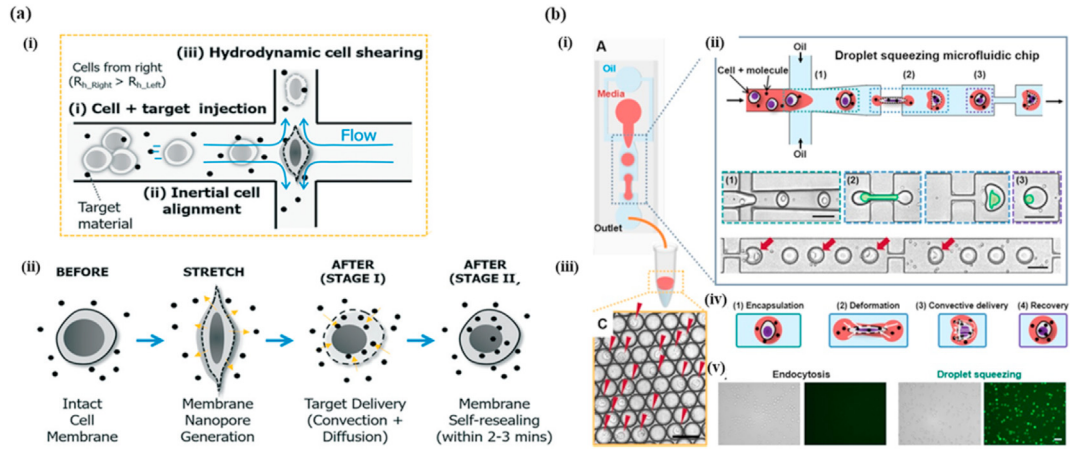

Fig. 14. (a) (i) Schematic and illustration of the proposed device and delivery methodology. (ii) Illustration of cell stretching, transient pore generation, biomolecular delivery, and resealing. Reprint with permission from The Royal Society of Chemistry [50]. (b) Droplet squeezing platform. (i) Schematic of the microfluidic device. (ii) Illustration of delivery process along with high-speed microscope images, showing (1) encapsulation, (2) deformation, and (3) restoration. (iii) Single-cell encapsulated monodispersed droplets (cells indicated by red arrow). (iv) Illustration of droplet squeezing and cargo delivery by convection-based transport. (v) Bright-field and fluorescence images of endocytosis and droplet squeezing-mediated uptake of 3–5 kDa FITC-dextran into K562 cells after 18 h (Scale bar = 50 μm). Reprint with permission from the American Chemical Society [53].

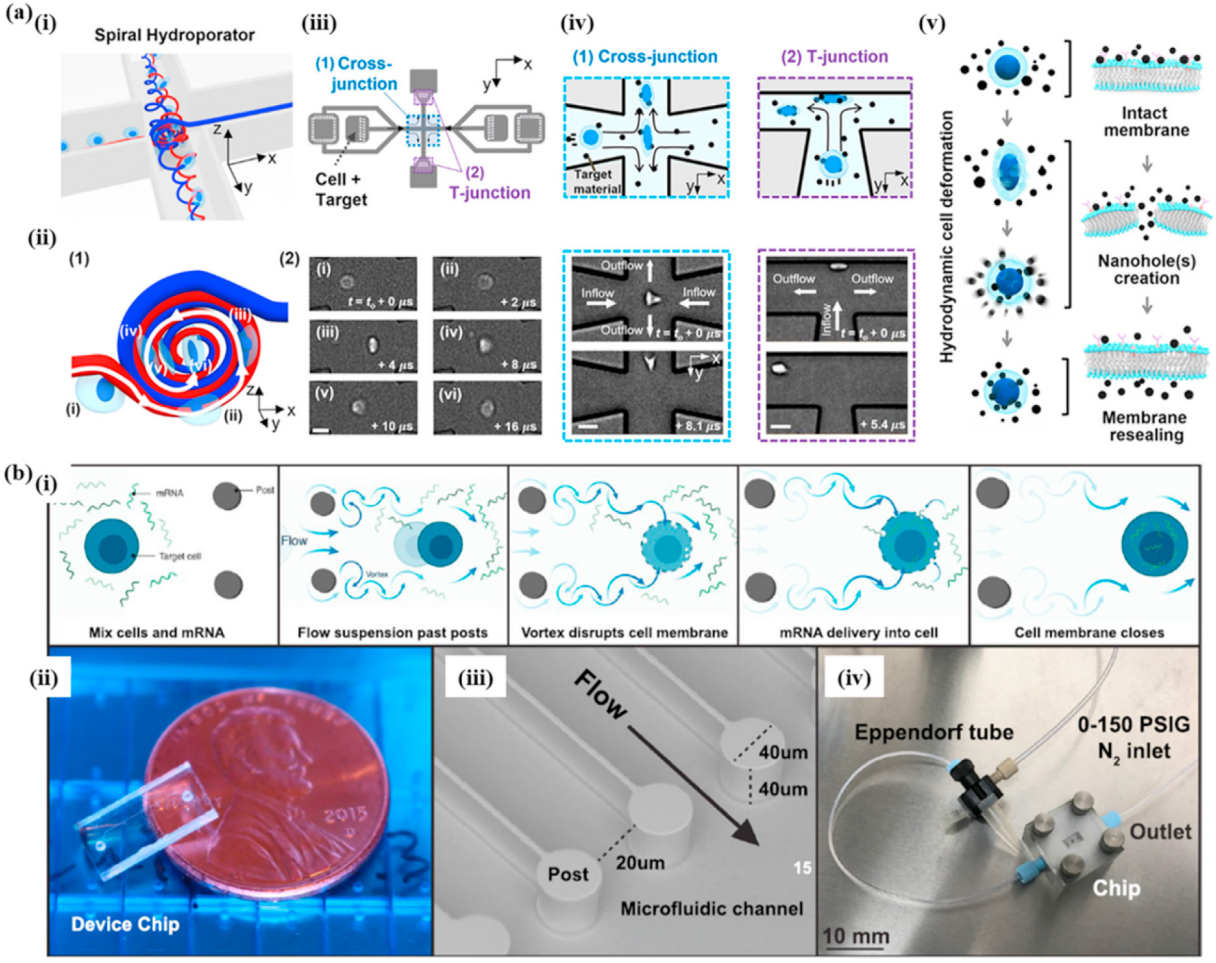

Fig. 15. (a) Hydroporation device employing spiral vortex flow. (i) Schematic of spiral flow at cross-junction. (ii) (1) Illustration of cell deformation using a spiral vortex. (2) Cell rotation at cross-junction captured using high-speed microscopy. (iii) Device design using computer-aided design (CAD). (iv) Cell deformation using hydrodynamic forces at the Cross junction and T-junction. (v) Illustration of nanomaterial delivery into the cell. Reprint with permission from the American Chemical Society [51]. (b) μVS device. (i) Schematic of the μVS-based delivery system (not to scale). (ii) Photographic image of the microfluidic chip. (iii) Image of microfluidic channel showing the flow direction, post dimensions, and post spacing (captured using SEM). (iv) Image of assorted hardware used to push cel, mRNA suspension through the chip. Reprint with permission from Scientific Reports Nature [52].

hydroporation. The design comprised a cross-junction and two T-junctions (Fig. 15(a)(iii)) and was fabricated using PDMS-molding. Cell-nanomaterial mixture was passed in with different flow rates through the opposing channels, and they subsequently exit through the T-junction (Fig. 15(a)(iv)). As a cell in this intersection region spirals around and approaches the stagnation point, they undergo asymmetric cell stretching, leading to transient pore formation and subsequent influx of nanomaterial from the surrounding (Fig. 15(a)(v)). The fluid inertia then guides the cell towards the T-junction walls, during which they undergo membrane recovery. At the T-junction wall, they collide once again to undergo deformation. The repeated collision recovery process leads to convective and diffusive delivery. Experimental results combined with previous literature suggested that an increase in the Re of the fluid flow from 0 to 366 led to the development of a strong spiral vortex at the crossing. At low values of Re, the fluid stream interface remains sharp and symmetric and up an above Re of 37.9 (critical Re), swirling motions dominate. The method demonstrated successful delivery of AuNPs, DOX-MSN (mesoporous silica nanoparticles loaded with doxorubicin), and mRNA in MDA-MB-231 and K-562 cells with high efficiency (up to 96.5%), high throughput ($\sim 10^6$ cells/min), and increased cell viability (up to 94%).

Jarrell et al. [52] positioned an array of equally spaced posts in a microfluidic device to generate hydrodynamic vortices. This was called a Microfluidic Vortex Shedding (μVS) device. The device was fabricated on fused silica wafers using anisotropic DRIE. As shown in Fig. 15(b)(i), when fluid flows past the array posts (at Re value greater than 40), vortices are generated, which induce cell membrane disruption and allow diffusion of mRNA into the cell. The distance between the 40 μm diameter posts can be adjusted from 10 to 40 μm depending on cell type and size (see Fig. 15(b)(iii)). Simulation results indicated an optimum Re value of 146 to sustain the vortices, which eventually reduced down at the end of the channel. Experimental results on human T cells when delivering mRNA at a concentration greater than 80 μgmL^{-1} demonstrated optimum transfection efficiency (63.6% peak) and cell viability (75–81%) – the values increased with increasing mRNA concentration. The method also ensured uniform EGFP expression in $CD4^+$ and $CD8^+$ human T cells as opposed to cell squeezing strategies which have expression biases. The total cell recovery rate is around 20%, which is almost 5-fold greater than the electroporation technique.

To summarize this, the hydroporation technique is a relatively new area of study with tremendous potential due to its low cost, extremely high throughput, high transfection efficiency, high cell viability and ease of operation, when compared to the previous methods. The clogging issues of mechanical confinement are significantly overcome, with improved results when transfecting large molecules. However, like mechanical confinement, the hydroporation technique is only limited to suspended cell types with the delivery process being greatly non-uniform, which may often restrict its usability.

The different microfluidic mechanoporation techniques such as microfluidic-based microinjection, micro/nanoneedles arrays, mechanical confinement, hydrodynamic manipulation, and their advantages, disadvantages, governing parameters and cellular analysis are provided in Table 1.

3. Integrated intracellular delivery strategies

The different mechanoporation platforms, as discussed in the previous section, have high transfection efficiencies with high cell viabilities when transfecting smaller biomolecules. Some of these platforms have also demonstrated throughputs of over 1 million cells per minute [40,51]. However, all the methods discussed above have some inherent disadvantages. For example, the delivery efficiencies of larger biomolecules and genetic material (DNA, siRNA) are generally low for all methods, except microinjection. Microinjection, despite its precision, suffers from lower throughput and complex machinery.

Other membrane disruption methods employing microfluidic-based strategies have often demonstrated excellent results for delivering specific cargo in cells. Electroporation, for example, has long held its dominance as the most effective tool for highly efficient transfection of large molecules into hard-to-transfect cell types [18,20] and as an efficient tool for cellular therapy and analysis [16]. Although they have obtained great success in efficiently transfecting DNA molecules across the cell membrane, the low cell viabilities often restrict their usage. This can be accounted to higher voltages applied and larger electrode surface area, which causes electrolysis. Magnetoporation is a very promising method for *in vivo* analysis. However, despite high cell viability, the low efficiency of magnetoporation platforms is a major disadvantage [30,31]. Photoporation platforms have high throughput and high efficiencies but often have low cell viabilities [23,25]. The different membrane disruption methods-based delivery strategies, such as electroporation, optoporation, magnetoporation, acoustoporation, mechanoporation, and their advantages and disadvantages, are provided in Table 2.

The specific advantages of these different membrane disruption methods have prompted many research groups to study the effect of combining the various membrane disruption techniques in a single microfluidic device. The results obtained have indicated significant improvement in cargo delivery when compared to using these membrane disruption methods alone. For example, previous studies [33,156] had indicated the ability of cavitation bubbles to enable cell membrane disruption. This idea was used in a photoporation platform called BLAST (biophotonic laser-assisted surgery tool) [22], where successful pumping of ultra-large cargo such as *F. novicida* bacterium into HeLa cells was obtained using light pulse, a first of its kind. Sonoporation in combination with electrophoretic insertion [157] demonstrated DNA transfection with high efficiency, which did not previously occur using only sonoporation [34]. Microneedle patches in combination with iontophoresis showed delivery of FITC-dextran (up to 200 kDa) [158] and insulin [159], which was not previously obtained using microneedles or iontophoresis alone.

For the mechanoporation-integrated delivery strategies, the developments have been divided into two sections; hybrid mechanoporation [72–75] and mechanoporation-inspired intracellular delivery [76–80]. While the former talks about the different designs that combine mechanoporation with other membrane-disruption based techniques, the latter discusses methods which have borrowed ideas from different mechanoporation concepts to design platforms, where biomolecular delivery essentially takes place by membrane disruption (non-mechanoporation) or carrier based techniques. The key inspiration for this section is to provide a new direction for readers and researchers to not merely treat the different transfection strategies as isolated and individual methods, but to correlate and/or derive ideas from the different existing techniques to create novel intracellular delivery devices. All of the methodologies discussed subsequently have demonstrated interesting and unique results, which were not obtained previously. They have been discussed in detail subsequently.

3.1. Hybrid mechanoporation

As mentioned previously, hybrid mechanoporation includes the delivery strategies, where cells are subjected to a combination of mechanical forces and other membrane-disruption delivery technique. The two methods work in tandem in a single device, and have the advantage of utilizing lesser extreme operational parameters than when they are used individually. This has led to enhanced delivery efficiencies and cell viabilities for these hybrid techniques, some of which are discussed below.

Microinjection has traditionally been used as a glass capillary-based, pressure-driven, cell-penetrating injection device [62]. While effective for small-sized biomolecules, restriction in the maximum permissible microinjector diameter limits the delivery of macromolecules [62,77]. Irreversible cell membrane damage due to improper needle insertion also limits cell viability. The penetration mechanism also requires strong structural support, which raises equipment costs. These specific

limitations have been overcome by different non-penetrating or partly penetrating methods such as lipid-assisted microinjection [76,160], electro-injection [72,73,161], and photothermal injection [77,162]. While electro-injection is discussed in this section, we review lipid-assisted microinjection and photothermal injection in the subsequent section.

Electro-injection was initially demonstrated by Karlsson et al. [72], where giant unilamellar vesicles (GUVs) were positioned between a micropipette injector (equipped with a Pt electrode) and a carbon fiber microelectrode (tip diameter = 5 μm). As shown in Fig. 16(a), as the injection tip moved towards the GUV, the resulting mechanical force resulted in the vesicle acquiring a kidney-like shape. An electric field (40 V/cm, 3 ms) was then applied through the microelectrode, which helped permeabilize the membrane and ensured needle insertion into the vesicle. Because of the electro-assisted injection procedure, the micropipette tip diameter could range up to 2.5 μm. This resulted in the delivery of various large-sized biopolymers and colloidal particles in unilamellar vesicles and a single PC12 cell. A subsequent study by Hurtig et al. [161] also showed the delivery of *E. coli* (MG1655 strain) in GUVs. A similar method by Shirakashi et al. [163] analyzed the electro-injection mechanism using medaka egg cells [164]. However, this approach of employing two opposite electrodes leads to highly non-localized membrane permeabilization.

To overcome this issue, Seger et al. [73] used a gold-sputtered double-barrel nanopipette, which was used in conjunction with a scanning ion conductance microscope (SICM) to locate the cell surface, where the nanopipette was inserted into the cytoplasm later (Fig. 16(b)(i)). One of the barrels was then biased with respect to the other, and the desired biomolecule was injected into the cytoplasm by the controlled voltage (10 V, 500 ms). The pipettes were fabricated from glass capillaries using a pipette puller [165]. Experiments using human BJ fibroblasts indicated successful delivery of carboxyfluorescein with over 70% cell viability. Independent injection of different dyes with controllable ratios was also demonstrated.

Development on the cell squeeze technique [40] was performed by Ding et al. [74]. As shown in Fig. 16(c), parallel microelectrodes were incorporated at the end of the constriction channels. This has been referred to as a disruption-and-field-enhanced (DFE) delivery. The cell squeezing method had not obtained much success in transfecting DNA molecules into the cell. Electroporation in this regard had demonstrated good results [166]. The device aimed at combining the high throughput delivery capability of cell squeezing with the efficacy of electroporation for rapid DNA transfection. Experiments to deliver plasmid DNA directly into the HeLa cell nucleus indicated DNA expression occurred in more than 80% of transfected cells within 1 h of treatment. This value is way greater than electroporation which demonstrated 70% efficiency only after 4–48 h. Although microinjection has achieved similar expression results as the DFE technique, the latter can perform it at a very high throughput (up to 10^6 cells per device per minute). The results suggested that DNA, mRNA transfection is majorly determined by the electric field while mechanical disruption governs the intracellular protein delivery.

Micro/nanorobots have been under research for over a decade, finding various *in vivo* cellular delivery, surgery, and sensing applications [167]. The robots can be manipulated using biological, chemical, acoustic, or magnetic actuation. Previous studies using magnetically actuated CNT nanospears had demonstrated good results by delivering in hard-to-transfect cells [30]. The CNT-nanospears platform was also efficient in repeated biomolecule extraction for cell monitoring [168]. However, issues related to the cytotoxicity of CNTs [169] required the development of biocompatible nanospears for cellular delivery and assessment. In this regard, Xu et al. [75] designed magnetically controlled nanospears (length ~ 5 μm, tip diameter <50 nm). PS particles on a Si substrate were used to fabricate the nanospears by combining oxygen plasma etching and reactive ion etching. A Ni layer (provides

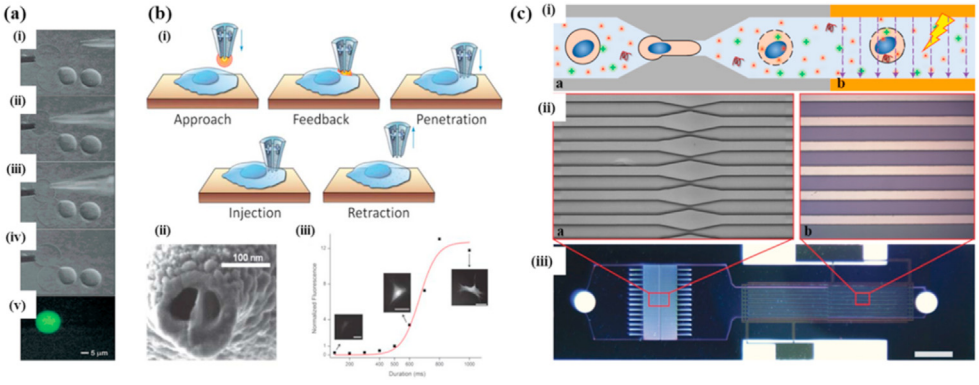

Fig. 16. (a) Electro-injection of fluorescein into GUV. (i) DIC image showing two adjacent unilamellar vesicles on the coverslip surface and two multilamellar liposomes. (ii) An applied mechanical force, changing the vesicle into a kidney-like shape by moving the injection tip on the vesicle and towards the microelectrode. (iii) Membrane permeabilization due to the applied electric field, consequent tip insertion fluorescein injection into the vesicle. (iv) The removal of injection tip and counter electrode from the vesicle. (v) Fluorescence image of an injected vesicle. Reprint with permission from the American Chemical Society [72]. (b) Double-barrel nanopipette. (i) Schematic of cell surface detection and subsequent injection using the double-barrel nanopipette. (ii) SEM image of the nanopipette. (iii) Normalized fluorescence intensity after injection. Reprint with permission from The Royal Society of Chemistry [73]. (c) DFE delivery device. (i) Schematic of device operation. a. Squeezing of cells as they pass through constriction channels. b. Cells being subjected to electric pulses that drive DNA into the cytoplasm and nucleus through the disrupted membrane. (ii) Magnified image of the DFE device. a. Identical and parallel constriction channels on a Si wafer for cell squeezing. b. Microelectrodes on a pyrex wafer for electroporation. (iii) Final device obtained by joining the Si and pyrex wafer. Reprint with permission from Springer Nature [74].

nanospears with magnetic properties due to its ferromagnetism) and an Au layer (serves as a surface for loading biomolecules) were deposited on it using e-beam evaporation to generate a Si/Ni/Au nanospear. Finally, nucleic acids (11-mercaptoundecanoic acid (MUA), polyethyleneimine (PEI), and eGFP-expression plasmids) were deposited sequentially to generate nanospears, encapsulated with MUA/PEI/eGFP-expression plasmids. The nanospears were subsequently magnetized, mechanically scraped off, and dispersed in the desired media. A sufficiently large magnetic field gradient enabled accurate control over the orientation, location, and speed of the nanospears. This magnetic field was used to guide these nanospears towards penetrating the target cell membrane and release the dissolved protein, as shown in Fig. 17. Experiments using approximately 200,000 U87 cells with around 1 million nanospears demonstrated high transfection efficiency (~80%) and high cell viability (>90%).

3.2. Mechanoporation-inspired intracellular delivery

Mechanoporation-inspired intracellular delivery techniques refer to those methodologies in which mechanical forces do not play a central role in device performance and cellular delivery. In the methods discussed subsequently, such as lipid-assisted microinjection [76], photothermal nanoblade [77], nanostraw/nanowire electroporation [78,79], nanostraw optoporation [80], transfection essentially takes place by other intracellular delivery techniques. However, to design these devices, key ideas from mechanoporation were re-imagined and integrated with other delivery techniques to create novel and highly efficient devices. The platforms, discussed subsequently, have demonstrated improved results than when these methods are used individually.

The simple lipid-assisted microinjection (SLAM) [76,160] uses a lipid-coated needle that gently contacts the target cell. The contact results in a fusion between the cell membrane and the lipid on the micropipette tip, forming a channel between the two, through which biomolecular delivery can take place. As opposed to a penetrating approach which demonstrated less than 5% viability when delivering Lucifer yellow in neutrophils, SLAM was able to achieve successful low pressure delivery with over 80% viability. Despite the results, unwanted toxicity arising out of cell-cargo lipophilic interactions [115] and longer time required for membrane-pipette fusion [170] can limit its usage.

Photothermal nanoblades, made of Ti-coated micropipettes, were developed by Wu et al. [77], where cell membrane deformation took place by explosive cavitation bubbles (Fig. 18(a)). The photothermal nanoblade (inner dia = 1.38 ± 0.1 μm, outer dia = 1.88 ± 0.1 μm) was fabricated using a heated and pulled capillary glass tube, where the Ti thin film (thickness = 102 ± 8 nm) was deposited at the tapered tip end using sputtering. As the nanoblade is made to contact a cell membrane gently, a nanosecond laser pulse is incident upon it, which causes the Ti (and consequently, the surrounding medium) to heat up, generating spatially patterned and temporally synchronized cavitation bubbles. The process triggers high-speed fluid flows and induces transient mechanical shear stress on the cell membrane, causing localized membrane cutting. Biomolecule delivery takes place simultaneously by a pressure-driven flow through the micropipette. Experiments demonstrated successful transfection of GFP-RNA in IMR90 (primary human lung fibroblasts) cells, 100 nm fluorescent PS beads (coated with DsRed lentiviral DNA) into hESCs, 200 nm fluorescent PS beads into HEK293T cells and B. thailandensis bacteria (0.7 μm × 2 μm) in HeLa cells. In particular, bacterial delivery occurred at an efficiency of ~46%. Cell viabilities were all greater than 90%. The platform was also successful in the direct nuclear delivery of DNA [162].

Xie et al. [78] developed the nanostraws device [39] to design a nanostraw-electroporation system (NES). In addition to the nanostraws (fabricated as discussed earlier in Section 2.2 [39,133]), the device had a platinum (Pt) electrode positioned in the cell culture well and an indium-tin-oxide (ITO) electrode coated below the fluidic channel, as shown in Fig. 18(b)(i). An electric field generated between the two electrodes passes through the nanostraws and permeabilizes the cells, where after biomolecular delivery takes place through the straws (Fig. 18(b)(ii)). Previous studies performed using only nanostraws indicated low delivery efficiency (~10%) when transfecting DNA plasmid [39]. The present study using nanostraws electroporation, however, achieved high plasmid transfection of 81% and 67% with application of minimal voltage (20 V, 200 μs, 200 pulses) using CHO cells and HEK293T cells, respectively. Cell viabilities were all above 98% and the platform also demonstrated effective co-transfection and sequential transfection of different DNA plasmids. Thus, nanostraws nanoinjection, when integrated with another membrane disruption method demonstrated enhanced intracellular delivery.

Subsequent experiments studied the effect of introducing different proteins into various cell types (including hard-to-transfect primary cells) using NES [171]. The results indicate that NES is a very effective platform for accurate control over the intracellular dosage, minimal perturbation with high controllability over the throughput [172]. Delivery of fluorescent nanodiamonds (FND) using NES has also been demonstrated [173]. The platform was also shown to be efficient in the non-destructive extraction and monitoring intracellular proteins and enzymes [174]. It can serve as a highly effective tool for analyzing circulating tumor cells (CTCs) [108]. The NES device fabrication was also modified to incorporate electroplated nanostraws, demonstrating promising results at lower voltages (~5 V) [175]. Delivery at far lower voltages (<2 V) with increased spatial precision [176] and enhanced visualization [177] was also achieved. Subsequent study using human primary T cells, by incorporating oscillatory mechanical stimulation with NES, resulted in a net transfection efficiency of 50% [178].

Messina et al. [80] developed organized plasmonic nanotubes, enabling intracellular delivery using controlled laser pulses. The nanostraw structure was fabricated using focused ion beam (FIB) milling on a silicon nitride membrane [179], and sputtering was performed for gold-coating the nanostraws structure. Short, focused, infrared laser pulses incident on the nanotubes led to plasmonic enhancement at the end of the nanotube (Fig. 19(a)(i)a). This led to local electron acceleration due to the enhanced electric field at the tip, generating shockwaves, which were sufficient to generate transient nanopores on the membrane of the cultured cells (Fig. 19(a)(i)b). Subsequently, diffusion-mediated biomolecular delivery takes place from the microfluidic chamber below (Fig. 19(a)(i)c), and the nanopores get sealed after approximately 10 min (Fig. 19(a)(i)d). Experiments of NIH3T3 cells using PI dye indicated very high delivery efficiency (>95%). The platform provides a very tight seal, preventing molecular uptake from the culture bath, allowing only biomolecules from the fluidic chamber underneath to pass through. Subsequent studies indicated the platform's ability to be used for the extracellular and intracellular recording of electrical activities [180,181], and single-particle delivery [177].

Microneedle-based electroporation devices had been previously studied for DNA, siRNA delivery into hard-to-transfect cells [182,183]. Although they demonstrated good results, plasmid delivery efficiencies were generally lower. To overcome this, very recently, triboelectric nanogenerator (TENG)-driven nanowire electrode arrays (NEA) were designed [79,184]. Two nanowire meshes were cylindrically rolled up and positioned coaxially in a sealed tube (containing the cells and target material), forming two electrodes, which were connected to the TENG terminals (Fig. 19(b)(i)). The copper oxide (CuO) nanowires were formed by oxidizing a Cu mesh in the air at 500 °C for 4 h (Fig. 19(b)(ii)). The TENG could generate open-circuit voltages of +115 V to −45 V (peak short circuit current ~ −5 to +15 μA) by simple human tapping motion (Fig. 19(b)(iv)). This enabled nanowire-assisted localized electroporation of cells and biomolecular delivery by cell poking and electro-transfection. Experiments using MiaPaCa-2 (pancreatic cancer cell line) and K-562 cells at a pulse duration of 40s, demonstrated siRNA delivery efficiencies of 95% and 84%, respectively, with high cell viability (>90%). The TENG-driven NEA (T-NEA) platforms are self-powered, with very simple operation procedure and have the advantage of being able to deliver

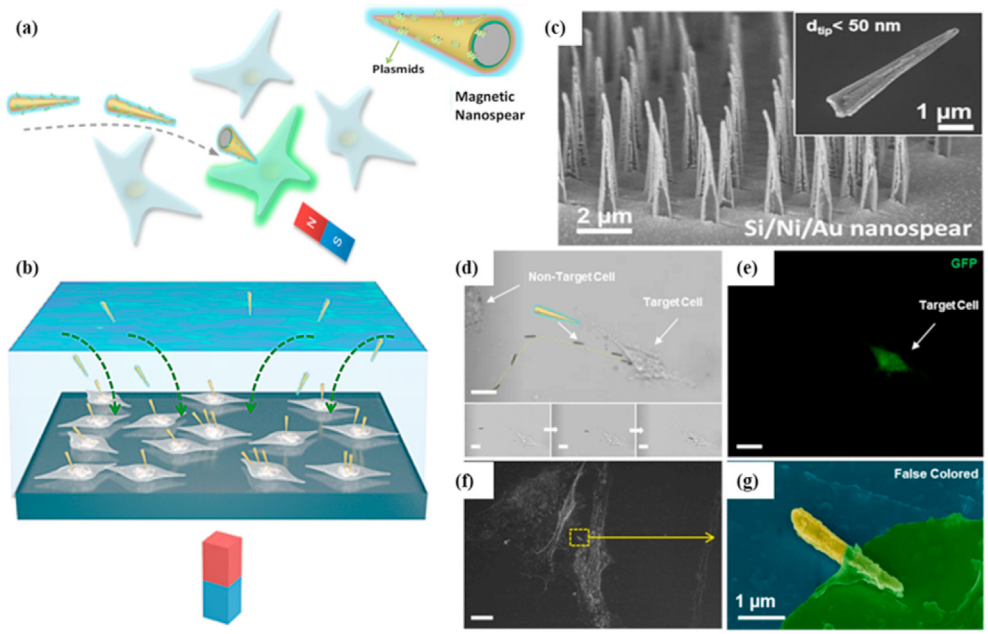

Fig. 17. Schematic of the magnetic nanospear-mediated delivery device. (a) Schematic of Si/Ni/Au nanospear encapsulated with eGFP-expression plasmid magnetically guided and inserted into a target cell. (b) Illustration of multiple nanospears for high-throughput transfection. (c) SEM image of nanospear arrays. (d) Image showing controlled trajectory of a single nanospear and targeted intracellular delivery (Scale bar = 10 μm). (e) GFP expression by target U87 cell were obtained using fluorescence microscopy 24 h after treatment (Scale bar = 10 μm). (f) SEM image of nanospears inside a target cell (Scale bar = 10 μm). (g) False colored, magnified SEM image of nanospears inside a target cell. Reprint with permission from the American Chemical Society [75].

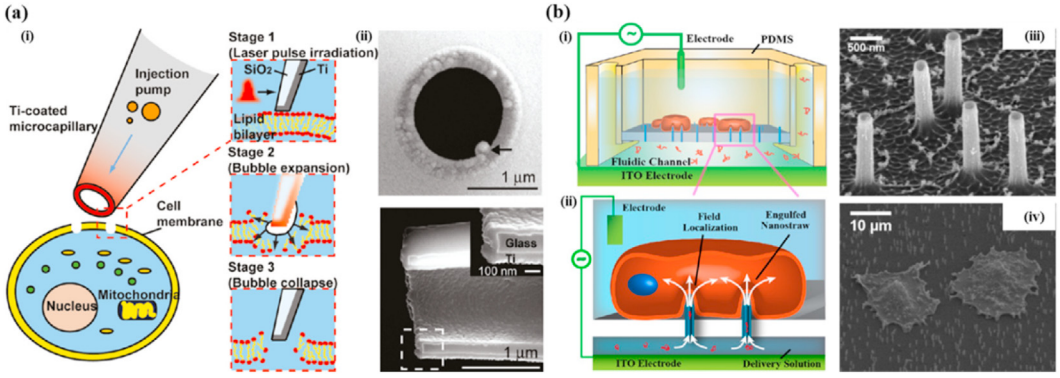

Fig. 18. (a) Photothermal nanoblade. (i) The different stages describing the mechanism for membrane cutting and cargo delivery. (ii) SEM image of the Ti-coated glass microcapillary pipette (The arrowhead is directed towards the glass filament edge, which is present inside the micropipette). Reprint with permission from the American Chemical Society [77]. (b) Nanostraw electroporation device. (i) Schematic of the device. (ii) Schematic of biomolecular delivery by field localization at the nanostraw tip. (iii) SEM image of nanostraws (diameter = 250 nm, array density = 0.2 straws/μm^2). (iv) SEM image of cells cultured on the nanostraws membrane. Reprint with permission from the American Chemical Society [78].

transdermally and *in vitro*. Thus, the T-NEA device can develop into a very significant platform for intracellular delivery and cellular analysis of hard-to-transfect adherent and suspended cell types [185].

The different integrated methods discussed in this section have all demonstrated excellent results in transfecting larger biomolecules, demonstrating highly efficient nuclear transfection with high cell viability. They have been summarized in Table 3.

4. Limitations and future prospects

The ultimate goal for any intracellular delivery platform is to develop a universal platform capable of transfecting any nanomedicine, peptides, molecular tags, etc. Some of the critical delivery parameters include high throughput, high transfection efficiency, uniform dosage control and negligible effect on cell viability. A major restriction of the current high throughput mechanoporation platforms is their inability to uniformly transfect the cells in a sample. Again, while micro/nanoneedle arrays have been mostly successful in transfecting adherent cell types, cell squeezing and hydroporation can only deliver to suspended cells. Each of these platforms also has some additional constraints.

Micro/nanostructure-mediated delivery has been successful in transfecting a wide range of biomolecules into various primary and patient-derived cell types. Yet, for solid nanostructures, as the biomolecules are often coated on the needle surface, the delivery can only be performed once. For repeated administration, the cells need to be detached and reattached again, hindering co-delivery of molecules. Hollow structures, on the other hand, are limited by continuous delivery of extracellular molecules from the fluidic chamber and continuous leakage of intracellular molecules to the external environment [2,92]. A major limitation of the cell squeezing platform is channel clogging. While cells flowing through a channel are already under high stress due to the fluid pressure, compressing them through channels only leads to additional stresses, inducing cell death. The subsequent cellular debris at the constriction leads to inconsistent operation, which effectively reduces throughput and induces fouling. Again, most of the mechanoporation platforms sparing hydroporation [47,49–53], have not achieved significant success in delivery of macromolecules and genetic materials.

In this regard, the integrated methods, such as those discussed in Section 3, have been developed significantly to transfect larger molecules, demonstrating highly efficient cellular as well as nuclear

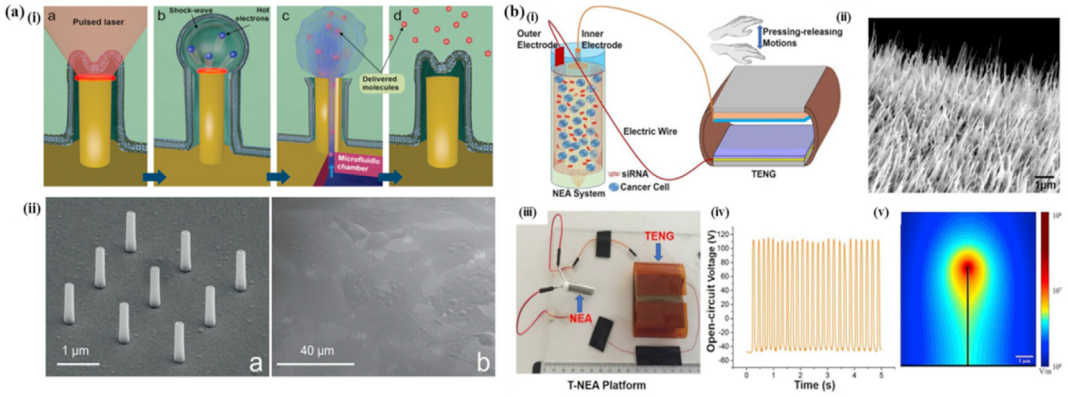

Fig. 19. (a) Nanostraw optoporation device. (i) Illustration of the delivery method using plasmonic nanotube. a. Excitation of nanotube by a laser pulse. b. Generation of transient nanopores by pressure waves. c. Intracellular biomolecule delivery through the nanopores. d. Closing down of nanopores. (ii) SEM images of a. 3 × 3 nanopillars array. b. NIH3T3 cells culture upon the nanotube array. Reprint with permission from WILEY-VCH Verlag GmbH & Co [80]. (b) T-NEA device. (i) Illustration of the experimental setup and siRNA delivery into suspended cell types. (ii) SEM image of the Cu-nanoarrays (length ~ 5 μm, diameter <50 nm, density ~ 10 nanowires/μm^2). (iii) Photograph of the T-NEA device. (iv) Open circuit voltage induced by human tapping motion on the TENG. (v) Electric field distribution simulation at a single CuO-nanowire tip. Reprint with permission from Elsevier [79].

Table 3
Comparison between various combinatory methods.

Sl. No.	Combinatory Technique		Working principle	Highlights	References
1.	Hybrid mechanoporation	Electro-injection	Combines electroporation with microinjection	– Low cell damage due to minimal needle penetration – Low pressure delivery – Larger needle diameter can be used – Lower electrical field parameters than conventional electroporation – Ability to precisely transfect macromolecules	[72,73,161, 163,164]
		Mechano-electroporation	Combines electroporation with cell squeezing	– High throughput delivery (~10^6 cells/min) of plasmid DNA (~80% delivery efficiency in 1hr) – Issues related to clogging are minimized since cells are not squeezed heavily – Lower electrical field parameters than conventional electroporation	[74]
		Magneto-mechanoporation	Magnetically-guided nanospears to pierce the cell membrane	– Delivery of plasmid DNA with high transfection efficiency (~80%) and cell viability (>90%) – Low transfection efficiency and lower cell viability, associated with conventional magnetoporation is overcome	[30,75,168, 169]
2.	Mechanoporation-inspired intracellular delivery	Lipid-assisted microinjection	Lipid-coated hollow microneedle in contact with cell membrane	– Low pressure delivery – Low cell damage due to no penetration – Independent of operator expertise	[76,160]
		Photothermal nanoblade	Ti-coated micropipettes in contact with cell membrane and exposed to nanosecond laser pulse	– Successful bacterial delivery (~46%) into mammalian cells – Low cell damage due to no penetration – Independent of operator expertise	[77,162]
		Nanostraw-electroporation	Electroporation using hollow nanoneedle array	– High plasmid transfection (~81%) with over 98% cell viability – Lower electrical field parameters than conventional electroporation – Co-transfection and sequential transfection of different DNA plasmids can be performed – Can be used for non-destructive extraction and monitoring of intracellular proteins and enzymes	[78,108,171, 173–177]
		Nanostraw optoporation	Optoporation using hollow nanoneedle array	– Intracellular delivery with over 95% efficiency – Can be used for extracellular and intracellular recording of electrical activities	[80,177,180, 181]
		Nanoneedle electroporation	Electroporation using solid nanoneedle array	– Enhanced throughput obtained – Highly efficient delivery of a variety of micro/macromolecules – T-NEA device can deliver both transdermally and *in vitro* – Self-powering ability of T-NEA device, makes it a promising candidate for wearable and personalized healthcare	[79,182–184]

transfection with high viability. High throughput mechano-electroporation strategies [74,78,79] have shown excellent results in macromolecular transfection. Of these, the self-powered TENG device [185] has immense potential to develop into a very dynamic platform for wearable and personalized healthcare. Again, the plasmonic, conductive nanotubes device [177] is one of the few platforms that can utilize the specific advantages of mechanoporation, electroporation, and photoporation for administering and monitoring biomolecules at a single-molecule level. Future developments can concentrate on incorporating the particular benefits of other intracellular delivery techniques to design truly multifunctional platforms which can independently or simultaneously deliver biomolecules at lesser extreme operational parameters.

Subsequent studies on mechanoporation should focus keenly on device optimization, targeting uniform and effective transfection across every cell type at high throughputs. The different processes can be automated and integrated with feedback systems to meet quality and control over the transfection. On an experimental level, different materials [186,187] can be studied to fabricate these microfluidic platforms with a focus on increased biocompatibility and reduced leakage [71,186]. Key emphasis should be put in making these platforms compatible with high resolution microscopy, to enable post-delivery assessment of stress responses and monitoring cellular functions. Also, most of the molecular probes used in experiments are either small-sized organic dyes or large antibodies. Subsequent research can, for example, emphasize on creating nanosensor probes, which can facilitate the study of intracellular microenvironment for applications in *in vivo* cell tracking [4]. An *in vivo* analysis is highly necessary to understand the physiological behavior of these mechanoporation devices and subsequently promote their clinical applications. It is noteworthy that majority of the works reviewed in this article are in their nascent stage, requiring further analysis to facilitate their use in the human body.

To conclude, the challenges to intracellular delivery and cellular analysis are highly interdisciplinary. To truly understand and formulate innovative solutions to existing challenges, a collaborative effort between doctors, medical professionals, pharmacologists, and engineers is of utmost importance. The objective should be to design low cost, versatile and GMP (good manufacturing practice)-compliant platforms, able to perform *in vivo* delivery, thereby enabling rapid clinical applications [71,188]. Designing clinically relevant outcomes is the ultimate goal of drug-delivery researchers, and it is only through a biologically instigated engineering approach that we can truly make significant leaps in developing simple, affordable, and clinically relevant devices for intracellular delivery and biological analysis [188,189].

5. Conclusion

Mechanoporation implies the deformation of the cell membrane by applying physical forces onto the cell. These forces lead to the formation of transient membrane pores, and macromolecular delivery takes place by simple diffusion or convection process. The earliest method was the microinjection technique which demonstrated delivery with high transfection efficiency and high cell viability, but with limited throughput and excessive operational cost. The advent of micro/nanotechnology led to increased interest in developing microfluidic devices for intracellular delivery as these platforms were low cost, biocompatible and enabled high throughput analysis of a variety of cell types. Microfluidic-based mechanoporation techniques such as microfluidic-based microinjection, microfluidic-based nanoneedle arrays, microfluidic device employing mechanical confinement, and microfluidic device employing hydrodynamic manipulation have consequently been developed. Microinjection and microneedle arrays-based techniques are generally low throughputs and high cost. However, this limitation is overcome by cell squeezing and hydroporation techniques, which possess very high throughput. With the increase in throughput, however, the efficiency in transfecting large molecules drastically decreases. Yet, combining mechanoporation with other methods such as electroporation or magnetoporation have significantly improved the transfection efficiency. However, significant development is still required to transfect ultra-large biomolecules, pathogens, etc., into various cell types. Some limitations can be overcome by employing a biologically initiated approach towards designing intracellular delivery platforms, focusing on gaining an in-depth understanding of the biomolecule-cell interaction. Nevertheless, the currently available microfluidic mechanoporation platforms are highly economic tools capable of effective intracellular delivery and cellular analysis.

Declaration of competing interest

The authors declare the following financial interests/personal relationships which may be considered as potential competing interests: Tuhin Subhra Santra reports financial support was provided by the DBT/Wellcome Trust India Alliance Fellowship.

Acknowledgement

This work was supported by the DBT/Wellcome Trust India Alliance Fellowship grant number IA/E/16/1/503062 awarded to Dr Tuhin Subhra Santra.

References

[1] M.P. Stewart, A. Sharei, X. Ding, G. Sahay, R. Langer, K.F. Jensen, In vitro and ex vivo strategies for intracellular delivery, Nature 538 (2016) 183–192, https://doi.org/10.1038/nature19764.
[2] J. Brooks, G. Minnick, P. Mukherjee, A. Jaberi, L. Chang, H.D. Espinosa, R. Yang, High throughput and highly controllable methods for in vitro intracellular delivery, Small (2020) 1–20, https://doi.org/10.1002/smll.202004917, 2004917.
[3] N. Rusk, Seamless delivery, Nat. Methods 8 (2011), https://doi.org/10.1038/nmeth.f.331, 44–44.
[4] J. Liu, J.C. Fraire, S.C. De Smedt, R. Xiong, K. Braeckmans, Intracellular labeling with extrinsic probes : delivery strategies and applications, Small (2020) 1–25, https://doi.org/10.1002/smll.202000146, 2000146.
[5] M.P. Stewart, R. Langer, K.F. Jensen, Intracellular delivery by membrane disruption: mechanisms, strategies, and concepts, Chem. Rev. 118 (2018) 7409–7531, https://doi.org/10.1021/acs.chemrev.7b00678.
[6] P.D. Robbins, S.C. Ghivizzani, Viral vectors for gene therapy, Pharmacol. Ther. 80 (1998) 35–47, https://doi.org/10.1016/S0163-7258(98)00020-5.
[7] W. Walther, U. Stein, Viral vectors for gene transfer, Drugs 60 (2000) 249–271, https://doi.org/10.2165/00003495-200060020-00002.
[8] C.E. Thomas, A. Ehrhardt, M.A. Kay, Progress and problems with the use of viral vectors for gene therapy, Nat. Rev. Genet. 4 (2003) 346–358, https://doi.org/10.1038/nrg1066.
[9] C. Pichon, L. Billiet, P. Midoux, Chemical vectors for gene delivery: uptake and intracellular trafficking, Curr. Opin. Biotechnol. 21 (2010) 640–645, https://doi.org/10.1016/j.copbio.2010.07.003.
[10] P. Midoux, C. Pichon, J.-J. Yaouanc, P.-A. Jaffrès, Chemical vectors for gene delivery: a current review on polymers, peptides and lipids containing histidine or imidazole as nucleic acids carriers, Br. J. Pharmacol. 157 (2009) 166–178, https://doi.org/10.1111/j.1476-5381.2009.00288.x.
[11] P. Shinde, A. Kumar, Kavitha, K. Dey, L. Mohan, S. Kar, T.K. Barik, J. Sharifi-Rad, M. Nagai, T.S. Santra, J. Shari, M. Nagai, T.S. Santra, Physical approaches for drug delivery : an overview, deliv. Drugs vol. 2 expect. Realities multifunct, Drug Deliv. Syst. (2020) 161–190, https://doi.org/10.1016/B978-0-12-817776-1.00007-9.
[12] P. Shinde, L. Mohan, A. Kumar, K. Dey, A. Maddi, A.N. Patananan, F.G. Tseng, H.Y. Chang, M. Nagai, T.S. Santra, Current trends of microfluidic single-cell technologies, Int. J. Mol. Sci. 19 (2018), https://doi.org/10.3390/ijms19103143.
[13] P.E. Boukany, A. Morss, W.C. Liao, B. Henslee, H. Jung, X. Zhang, B. Yu, X. Wang, Y. Wu, L. Li, K. Gao, X. Hu, X. Zhao, O. Hemminger, W. Lu, G.P. Lafyatis, L.J. Lee, Nanochannel electroporation delivers precise amounts of biomolecules into living cells, Nat. Nanotechnol. 6 (2011) 747–754, https://doi.org/10.1038/nnano.2011.164.
[14] T.S. Santra, S. Kar, H.Y. Chang, F.G. Tseng, Nano-localized single-cell nano-electroporation, Lab Chip 20 (2020) 4194–4204, https://doi.org/10.1039/d0lc00712a.
[15] T.S. Santra, Teitell M., Chiou P.Y., M.A. Teitell, P.E. Chiou, Device for massively parallel high throughput single cell electroporation and uses thereof, US Patent application No. 62/372, 743, 2018. https://patents.google.com/patent/US20180066222A1/en.
[16] B. Geboers, H.J. Scheffer, P.M. Graybill, A.H. Ruarus, S. Nieuwenhuizen, R.S. Puijk, P.M. van den Tol, R.V. Davalos, B. Rubinsky, T.D. de Gruijl, D. Miklavčič, M.R. Meijerink, High-voltage electrical pulses in oncology: irreversible electroporation, electrochemotherapy, gene electrotransfer, electrofusion, and electroimmunotherapy, Radiology 295 (2020) 254–272, https://doi.org/10.1148/radiol.2020192190.

[17] T.S. Santra, F.-G. Tseng, Electroporation for single-cell analysis, in: Essentials Single-Cell Anal., Springer-Verlag, Berlin Heidelberg, Germany, 2016, pp. 55–83, https://doi.org/10.1007/978-3-662-49118-8_3.
[18] J. Shi, Y. Ma, J. Zhu, Y. Chen, Y. Sun, Y. Yao, Z. Yang, J. Xie, A review on electroporation-based intracellular delivery, Molecules 23 (2018), https://doi.org/10.3390/molecules23113044.
[19] T.S. Santra, F.G. Tseng, Recent trends on micro/nanofluidic single cell electroporation, Micromachines 4 (2013) 333–356, https://doi.org/10.3390/mi4030333.
[20] S. Kar, M. Loganathan, K. Dey, P. Shinde, H.Y. Chang, M. Nagai, T.S. Santra, Single-cell electroporation: current trends, applications and future prospects, J. Micromech. Microeng. 28 (2018) 123002, https://doi.org/10.1088/1361-6439/aae5ae.
[21] D. Zhao, D. Huang, Y. Li, M. Wu, W. Zhong, Q. Cheng, X. Wang, Y. Wu, X. Zhou, Z. Wei, Z. Li, Z. Liang, A flow-through cell electroporation device for rapidly and efficiently transfecting massive amounts of cells in vitro and ex vivo, Sci. Rep. 6 (2016) 18469, https://doi.org/10.1038/srep18469.
[22] Y.C. Wu, T.H. Wu, D.L. Clemens, B.Y. Lee, X. Wen, M.A. Horwitz, M.A. Teitell, P.Y. Chiou, Massively parallel delivery of large cargo into mammalian cells with light pulses, Nat. Methods 12 (2015) 439–444, https://doi.org/10.1038/nmeth.3357.
[23] T.S. Santra, S. Kar, T.-C.C. Chen, C.-W.W. Chen, J. Borana, M.-C.C. Lee, F.-G.G. Tseng, Near-infrared nanosecond-pulsed laser-activated highly efficient intracellular delivery mediated by nano-corrugated mushroom-shaped gold-coated polystyrene nanoparticles, Nanoscale 12 (2020) 12057–12067, https://doi.org/10.1039/D0NR01792B.
[24] L. Mohan, S. Kar, M. Nagai, T.S. Santra, Electrochemical fabrication of TiO2 micro-flowers for an efficient intracellular delivery using nanosecond light pulse, Mater. Chem. Phys. 267 (2021) 124604, https://doi.org/10.1016/j.matchemphys.2021.124604.
[25] L. Mohan, S. Kar, P.S. Mahapatra, M. Nagai, T.S. Santra, Fabrication of TiO2microspikes for highly efficient intracellular delivery by pulse laser-assisted photoporation, RSC Adv. 11 (2021) 9336–9348, https://doi.org/10.1039/d0ra09785c.
[26] P. Shinde, S. Kar, M. Loganathan, H.Y. Chang, F.G. Tseng, M. Nagai, T.S. Santra, Infrared pulse laser-activated highly efficient intracellular delivery using titanium microdish device, ACS Biomater. Sci. Eng. 6 (2020) 5645–5652, https://doi.org/10.1021/acsbiomaterials.0c00785.
[27] H.A. Rendall, R.F. Marchington, B.B. Praveen, G. Bergmann, Y. Arita, A. Heisterkamp, F.J. Gunn-Moore, K. Dholakia, High-throughput optical injection of mammalian cells using a Bessel light beam, Lab Chip 12 (2012) 4816, https://doi.org/10.1039/c2lc40708f.
[28] P. Gupta, S. Kar, A. Kumar, F.-G. Tseng, S. Pradhan, P.S. Mahapatra, T.S. Santra, Pulsed laser assisted high-throughput intracellular delivery in hanging drop based three dimensional cancer spheroids, Analyst 146 (2021) 4756–4766, https://doi.org/10.1039/D0AN02432E.
[29] M. Arruebo, R. Fernández-Pacheco, M.R. Ibarra, J. Santamaría, Magnetic nanoparticles for drug delivery, Nano Today 2 (2007) 22–32, https://doi.org/10.1016/S1748-0132(07)70084-1.
[30] D. Cai, J.M. Mataraza, Z.H. Qin, Z. Huang, J. Huang, T.C. Chiles, D. Carnahan, K. Kempa, Z. Ren, Highly efficient molecular delivery into mammalian cells using carbon nanotube spearing, Nat. Methods 2 (2005) 449–454, https://doi.org/10.1038/nmeth761.
[31] S.N. Moysidis, K. Alvarez-Delfin, V.J. Peschansky, E. Salero, A.D. Weisman, A. Bartakova, G.A. Raffa, R.M. Merkhofer, K.E. Kador, N.J. Kunzevitzky, J.L. Goldberg, Magnetic field-guided cell delivery with nanoparticle-loaded human corneal endothelial cells, Nanomed. Nanotechnol. Biol. Med. 11 (2015) 499–509, https://doi.org/10.1016/j.nano.2014.12.002.
[32] H.D. Liang, J. Tang, M. Halliwell, Sonoporation, drug delivery, and gene therapy, Proc. Inst. Mech. Eng. Part H J. Eng. Med. 224 (2010) 343–361, https://doi.org/10.1243/09544119JEIM565.
[33] C.-D. Ohl, M. Arora, R. Ikink, N. de Jong, M. Versluis, M. Delius, D. Lohse, Sonoporation from jetting cavitation bubbles, Biophys. J. 91 (2006) 4285–4295, https://doi.org/10.1529/biophysj.105.075366.
[34] V.G. Zarnitsyn, J.M. Meacham, M.J. Varady, C. Hao, F.L. Degertekin, A.G. Fedorov, Electrosonic ejector microarray for drug and gene delivery, Biomed, Microdevices 10 (2008) 299–308, https://doi.org/10.1007/s10544-007-9137-4.
[35] S. Ramesan, A.R. Rezk, C. Dekiwadia, C. Cortez-Jugo, L.Y. Yeo, Acoustically-mediated intracellular delivery, Nanoscale 10 (2018) 13165–13178, https://doi.org/10.1039/c8nr02898b.
[36] A. Adamo, K.F. Jensen, Microfluidic based single cell microinjection, Lab Chip 8 (2008) 1258–1261, https://doi.org/10.1039/b803212b.
[37] X. Liu, Y. Sun, Microfabricated glass devices for rapid single cell immobilization in mouse zygote microinjection, Biomed. Microdevices 11 (2009) 1169–1174, https://doi.org/10.1007/s10544-009-9333-5.
[38] D. Huang, D. Zhao, J. Li, Y. Wu, L. Du, X. Xia, X. Li, Y. Deng, Z. Li, Y. Huang, Continuous vector-free gene transfer with a novel microfluidic chip and nanoneedle array, Curr. Drug Deliv. 16 (2018) 164–170, https://doi.org/10.2174/1567201815666181017095044.
[39] J.J. Vandersarl, A.M. Xu, N.A. Melosh, Nanostraws for direct fluidic intracellular access, Nano Lett. 12 (2012) 3881–3886, https://doi.org/10.1021/nl204051v.
[40] A. Sharei, J. Zoldan, A. Adamo, W.Y. Sim, N. Cho, E. Jackson, S. Mao, S. Schneider, M.-J. Han, A. Lytton-Jean, P.A. Basto, S. Jhunjhunwala, J. Lee, D.A. Heller, J.W. Kang, G.C. Hartoularos, K.-S. Kim, D.G. Anderson, R. Langer, K.F. Jensen, A vector-free microfluidic platform for intracellular delivery, Proc. Natl. Acad. Sci. Unit. States Am. 110 (2013) 2082–2087, https://doi.org/10.1073/pnas.1218705110.
[41] A. Liu, M. Islam, N. Stone, V. Varadarajan, J. Jeong, S. Bowie, P. Qiu, E.K. Waller, A. Alexeev, T. Sulchek, Microfluidic generation of transient cell volume exchange for convectively driven intracellular delivery of large macromolecules, Mater. Today 21 (2018) 703–712, https://doi.org/10.1016/j.mattod.2018.03.002.
[42] H. Xin, L. Zongbin, J.M. Chan, Z. Kai, L. Ying, Z. Zihua, L. Nan, Z. Youli, Q. Lidong, CRISPR-Cas9 delivery to hard-to-transfect cells via membrane deformation, Sci. Adv. 1 (2021), e1500454, https://doi.org/10.1126/sciadv.1500454.
[43] S. Modaresi, S. Pacelli, S. Subham, K. Dathathreya, A. Paul, Intracellular delivery of exogenous macromolecules into human mesenchymal stem cells by double deformation of the plasma membrane, Adv. Ther. 3 (2020) 1900130, https://doi.org/10.1002/adtp.201900130.
[44] X. Xing, Y. Pan, L. Yobas, A low-backpressure single-cell point constriction for cytosolic delivery based on rapid membrane deformations, Anal. Chem. 90 (2018) 1836–1844, https://doi.org/10.1021/acs.analchem.7b03864.
[45] R. Hao, Z. Yu, J. Du, S. Hu, C. Yuan, H. Guo, Y. Zhang, H. Yang, A high-throughput nanofluidic device for exosome nanoporation to develop cargo delivery vehicles, Small 17 (2021) 1–12, https://doi.org/10.1002/smll.202102150.
[46] A. Adamo, O. Roushdy, R. Dokov, A. Sharei, K.F. Jensen, Microfluidic jet injection for delivering macromolecules into cells, J. Micromech. Microeng. 23 (2013), https://doi.org/10.1088/0960-1317/23/3/035026.
[47] Y. Deng, M. Kizer, M. Rada, J. Sage, X. Wang, D. Cheon, A.J. Chung, Intracellular delivery of nanomaterials via an inertial microfluidic cell hydroporator, Nano Lett. 18 (2018) 2705–2710, https://doi.org/10.1021/acs.nanolett.8b00704.
[48] Q.T. Aten, B.D. Jensen, S.H. Burnett, L.L. Howell, A self-reconfiguring metamorphic nanoinjector for injection into mouse zygotes, Rev. Sci. Instrum. 85 (2014), https://doi.org/10.1063/1.4872077.
[49] J. Hur, I. Park, K.M. Lim, J. Doh, S.-G. Cho, A.J. Chung, Microfluidic cell stretching for highly effective gene delivery into hard-to-transfect primary cells, ACS Nano 14 (2020) 15094–15106, https://doi.org/10.1021/acsnano.0c05169.
[50] M.E. Kizer, Y. Deng, G. Kang, P.E. Mikael, X. Wang, A.J. Chung, Hydroporator: a hydrodynamic cell membrane perforator for high-throughput vector-free nanomaterial intracellular delivery and DNA origami biostability evaluation, Lab Chip 19 (2019) 1747–1754, https://doi.org/10.1039/c9lc00041k.
[51] G. Kang, D.W. Carlson, T.H. Kang, S. Lee, S.J. Haward, I. Choi, A.Q. Shen, A.J. Chung, Intracellular nanomaterial delivery via spiral hydroporation, ACS Nano 14 (2020) 3048–3058, https://doi.org/10.1021/acsnano.9b07930.
[52] J.A. Jarrell, A.A. Twite, K.H.W.J. Lau, M.N. Kashani, A.A. Lievano, J. Acevedo, C. Priest, J. Nieva, D. Gottlieb, R.S. Pawell, Intracellular delivery of mRNA to human primary T cells with microfluidic vortex shedding, Sci. Rep. 9 (2019) 3214, https://doi.org/10.1038/s41598-019-40147-y.
[53] B. Joo, J. Hur, G. Kim, S.G. Yun, A.J. Chung, Highly efficient transfection of human primary T lymphocytes using droplet-enabled mechanoporation, ACS Nano 15 (2021) 12888–12898, https://doi.org/10.1021/acsnano.0c10473.
[54] Yanyan Zhang, C.B. Ballas, M.P. Rao, Towards ultrahigh throughput microinjection: MEMS-based massively-parallelized mechanoporation, in: 2012 Annu. Int. Conf. IEEE Eng. Med. Biol. Soc., IEEE, 2012, pp. 594–597, https://doi.org/10.1109/EMBC.2012.6346001.
[55] Y.T. Chow, S. Chen, C. Liu, C. Liu, L. Li, C.W.M. Kong, S.H. Cheng, R.A. Li, D. Sun, A high-throughput automated microinjection system for human cells with small size, IEEE/ASME Trans. Mechatronics. 21 (2016) 838–850, https://doi.org/10.1109/TMECH.2015.2476362.
[56] S.J. Paik, S. Byun, J.M. Lim, Y. Park, A. Lee, S. Chung, J. Chang, K. Chun, D. Cho, In-plane single-crystal-silicon microneedles for minimally invasive microfluid systems, Sensors Actuators, A Phys. 114 (2004) 276–284, https://doi.org/10.1016/j.sna.2003.12.029.
[57] U.O. Häfeli, A. Mokhtari, D. Liepmann, B. Stoeber, In vivo evaluation of a microneedle-based miniature syringe for intradermal drug delivery, Biomed. Microdevices 11 (2009) 943–950, https://doi.org/10.1007/s10544-009-9311-y.
[58] C. Yeung, S. Chen, B. King, H. Lin, K. King, F. Akhtar, G. Diaz, B. Wang, J. Zhu, W. Sun, A. Khademhosseini, S. Emaminejad, A 3D-printed microfluidic-enabled hollow microneedle architecture for transdermal drug delivery, Biomicrofluidics 13 (2019) 64125, https://doi.org/10.1063/1.5127778.
[59] Y. Wang, Y. Yang, L. Yan, S.Y. Kwok, W. Li, Z. Wang, X. Zhu, G. Zhu, W. Zhang, X. Chen, P. Shi, Poking cells for efficient vector-free intracellular delivery, Nat. Commun. 5 (2014) 1–9, https://doi.org/10.1038/ncomms5466.
[60] D. Matsumoto, R. Rao Sathuluri, Y. Kato, Y.R. Silberberg, R. Kawamura, F. Iwata, T. Kobayashi, C. Nakamura, R.R. Sathuluri, Y. Kato, Y.R. Silberberg, Oscillating high-aspect-ratio monolithic silicon nanoneedle array enables efficient delivery of functional bio-macromolecules into living cells, Sci. Rep. 5 (2015) 3–5, https://doi.org/10.1038/srep15325.
[61] M.A. Barber, A technic for the inoculation of bacteria and other substances into living cells, J. Infect. Dis. 8 (1911) 348–360, https://doi.org/10.1093/infdis/8.3.348.
[62] M.M. Shanmugam, T.S. Santra, Microinjection for Single-Cell Analysis, Springer, Berlin, Heidelberg, 2016, pp. 85–129, https://doi.org/10.1007/978-3-662-49118-8_4.
[63] T.S. Santra, Microfluidics and Bio-MEMS: Devices and Applications, Jenny Stanford Publishing, 2020. https://books.google.co.in/books?id=RgsHEAAAQBAJ.
[64] T.S. Santra, F.-G.G. Tseng, Micro/Nanofluidic Devices for Single Cell Analysis, 2014, https://doi.org/10.3390/mi5020154.
[65] K. Kaladharan, A. Kumar, P. Gupta, K. Illath, T.S. Santra, F.-G. Tseng, Microfluidic based physical approaches towards single-cell intracellular delivery and analysis, Micromachines 12 (2021), https://doi.org/10.3390/mi12060631.

[66] J. Hur, A.J. Chung, Microfluidic and nanofluidic intracellular delivery, Adv. Sci. 8 (2021), https://doi.org/10.1002/advs.202004595.

[67] T.S. Santra, F.-G. Tseng, Single-cell analysis, Cells 9 (2020), https://doi.org/10.3390/cells9091993, 1993.

[68] T.S. Santra, F.-G. Tseng, Tuhin Subhra Santra, Fan-Gang Tseng, Handbook of Single Cell Technologies, Springer Singapore, 2019, https://doi.org/10.1007/978-981-10-4857-9.

[69] F.T. Tuhin, S. Santra, F. Prospects, Essentials of Single-Cell Analysis, Springer Berlin Heidelberg, Berlin, Heidelberg, 2016, https://doi.org/10.1007/978-3-662-49118-8.

[70] F. Tseng, T.S. Santra, Single Cell Analysis in Biotechnology and Systems Biology, MDPI, 2016, https://doi.org/10.3390/books978-3-03842-194-8.

[71] B. Duckert, S. Vinkx, D. Braeken, M. Fauvart, Single-cell transfection technologies for cell therapies and gene editing, J. Contr. Release 330 (2021) 963–975, https://doi.org/10.1016/j.jconrel.2020.10.068.

[72] M. Karlsson, K. Nolkrantz, M.J. Davidson, A. Stromberg, F. Ryttsen, B. Akerman, O. Orwar, Electroinjection of colloid particles and biopolymers into single unilamellar liposomes and cells for bioanalytical applications, Anal. Chem. 72 (2000) 5857–5862, https://doi.org/10.1021/ac0003246.

[73] R. Adam Seger, P. Actis, C. Penfold, M. Maalouf, B. Vilozny, N. Pourmand, Voltage controlled nano-injection system for single-cell surgery, Nanoscale 4 (2012) 5843, https://doi.org/10.1039/c2nr31700a.

[74] X. Ding, M.P. Stewart, A. Sharei, J.C. Weaver, R.S. Langer, K.F. Jensen, High-throughput nuclear delivery and rapid expression of DNA via mechanical and electrical cell-membrane disruption, Nat. Biomed. Eng. 1 (2017) 39, https://doi.org/10.1038/s41551-017-0039.

[75] X. Xu, S. Hou, N. Wattanatorn, F. Wang, Q. Yang, C. Zhao, X. Yu, H.-R. Tseng, S.J. Jonas, P.S. Weiss, Precision-guided nanospears for targeted and high-throughput intracellular gene delivery, ACS Nano 12 (2018) 4503–4511, https://doi.org/10.1021/acsnano.8b00763.

[76] I. Laffafian, M.B. Hallett, Lipid-assisted microinjection: introducing material into the cytosol and membranes of small cells, Biophys. J. 75 (1998) 2558–2563, https://doi.org/10.1016/S0006-3495(98)77700-8.

[77] T.H. Wu, T. Teslaa, S. Kalim, C.T. French, S. Moghadam, R. Wall, J.F. Miller, O.N. Witte, M.A. Teitell, P.Y. Chiou, Photothermal nanoblade for large cargo delivery into mammalian cells, 2011 16th Int. Solid-State Sensors, Actuators Microsystems Conf. TRANSDUCERS'11. (2011) 1813–1816, https://doi.org/10.1109/TRANSDUCERS.2011.5969731.

[78] X. Xie, A.M. Xu, S. Leal-Ortiz, Y. Cao, C.C. Garner, N.A. Melosh, Nanostraw–electroporation system for highly efficient intracellular delivery and transfection, ACS Nano 7 (2013) 4351–4358, https://doi.org/10.1021/nn400874a.

[79] C. Yang, G. Yang, Q. Ouyang, S. Kuang, P. Song, G. Xu, D.P. Poenar, G. Zhu, K.T. Yong, Z.L. Wang, Nanowire-array-based gene electro-transfection system driven by human-motion operated triboelectric nanogenerator, Nano Energy 64 (2019), https://doi.org/10.1016/j.nanoen.2019.103901.

[80] G.C. Messina, M. Dipalo, R. La Rocca, P. Zilio, V. Caprettini, R. Proietti Zaccaria, A. Toma, F. Tantussi, L. Berdondini, F. De Angelis, Spatially, temporally, and quantitatively controlled delivery of broad range of molecules into selected cells through plasmonic nanotubes, Adv. Mater. 27 (2015) 7145–7149, https://doi.org/10.1002/adma.201503252.

[81] S. Permana, E. Grant, G.M. Walker, J.A. Yoder, A review of automated microinjection systems for single cells in the embryogenesis stage, IEEE/ASME Trans. Mechatronics. 21 (2016) 2391–2404, https://doi.org/10.1109/TMECH.2016.2574871.

[82] Y. Zhang, L.-C.C. Yu, Single-cell microinjection technology in cell biology, Bioessays 30 (2008) 606–610, https://doi.org/10.1002/bies.20759.

[83] Q. Xu, Review of microinjection systems, in: Q. Xu (Ed.), Micromachines Biol. Micromanipulation, Springer International Publishing, Cham, 2018, pp. 15–47, https://doi.org/10.1007/978-3-319-74621-0_2.

[84] Z. Chi, Q. Xu, L. Zhu, A review of recent advances in robotic cell microinjection, IEEE Access 8 (2020) 8520–8532, https://doi.org/10.1109/ACCESS.2020.2964305.

[85] K. Van Der Maaden, W. Jiskoot, J. Bouwstra, Microneedle technologies for (trans) dermal drug and vaccine delivery, J. Contr. Release 161 (2012) 645–655, https://doi.org/10.1016/j.jconrel.2012.01.042.

[86] K. van der Maaden, R. Luttge, P.J. Vos, J. Bouwstra, G. Kersten, I. Ploemen, Microneedle-based drug and vaccine delivery via nanoporous microneedle arrays, Drug Deliv. Transl. Res. 5 (2015) 397–406, https://doi.org/10.1007/s13346-015-0238-y.

[87] A. Tay, N. Melosh, Nanostructured materials for intracellular cargo delivery, Acc. Chem. Res. 52 (2019) 2462–2471, https://doi.org/10.1021/acs.accounts.9b00272.

[88] G. He, N. Hu, A.M. Xu, X. Li, Y. Zhao, X. Xie, Nanoneedle platforms: the many ways to pierce the cell membrane, Adv. Funct. Mater. 30 (2020), https://doi.org/10.1002/adfm.201909890.

[89] S.T. Sanjay, W. Zhou, M. Dou, H. Tavakoli, L. Ma, F. Xu, X. Li, Recent advances of controlled drug delivery using microfluidic platforms, Adv. Drug Deliv. Rev. 128 (2018) 3–28, https://doi.org/10.1016/j.addr.2017.09.013.

[90] S. Henry, D. V McAllister, M.G. Allen, M.R. Prausnitz, Microfabricated microneedles: a novel approach to transdermal drug delivery, J. Pharmacol. Sci. 87 (1998) 922–925, https://doi.org/10.1021/js980042+.

[91] M.R. Prausnitz, Microneedles for transdermal drug delivery, Adv. Drug Deliv. Rev. 56 (2004) 581–587, https://doi.org/10.1016/j.addr.2003.10.023.

[92] Y. Chen, J. Wang, X. Li, N. Hu, N.H. Voelcker, X. Xie, R. Elnathan, Emerging roles of 1D vertical nanostructures in orchestrating immune cell functions, Adv. Mater. 32 (2020) 1–25, https://doi.org/10.1002/adma.202001668.

[93] Y.-C. Kim, J.-H. Park, M.R. Prausnitz, Microneedles for drug and vaccine delivery, Adv. Drug Deliv. Rev. 64 (2012) 1547–1568, https://doi.org/10.1016/j.addr.2012.04.005.

[95] S. Lee, W. Jeong, D.J. Beebe, Microfluidic valve with cored glass microneedle for microinjection, Lab Chip 3 (2003) 164–167, https://doi.org/10.1039/B305692A.

[96] T.E. McKnight, A.V. Melechko, G.D. Griffin, M.A. Guillorn, V.I. Merkulov, F. Serna, D.K. Hensley, M.J. Doktycz, D.H. Lowndes, M.L. Simpson, Intracellular integration of synthetic nanostructures with viable cells for controlled biochemical manipulation, Nanotechnology 14 (2003) 551–556, https://doi.org/10.1088/0957-4484/14/5/313.

[97] A.K. Shalek, J.T. Robinson, E.S. Karp, J.S. Lee, D.-R. Ahn, M.-H. Yoon, A. Sutton, M. Jorgolli, R.S. Gertner, T.S. Gujral, G. MacBeath, E.G. Yang, H. Park, Vertical silicon nanowires as a universal platform for delivering biomolecules into living cells, Proc. Natl. Acad. Sci. Unit. States Am. 107 (2010) 1870–1875, https://doi.org/10.1073/pnas.0909350107.

[98] C. Chiappini, E. De Rosa, J.O. Martinez, X. Liu, J. Steele, M.M. Stevens, E. Tasciotti, Biodegradable silicon nanoneedles delivering nucleic acids intracellularly induce localized in vivo neovascularization, Nat. Mater. 14 (2015) 532–539, https://doi.org/10.1038/nmat4249.

[99] S. Zappe, M. Fish, M.P. Scott, O. Solgaard, Automated MEMS-based Drosophila embryo injection system for high-throughput RNAi screens, Lab Chip 6 (2006) 1012–1019, https://doi.org/10.1039/b600238b.

[100] D. Delubac, C.B. Highley, M. Witzberger-Krajcovic, J.C. Ayoob, E.C. Furbee, J.S. Minden, S. Zappe, Microfluidic system with integrated microinjector for automated Drosophila embryo injection, Lab Chip 12 (2012) 4911–4919, https://doi.org/10.1039/C2LC40104E.

[101] X. Zhao, F. Xu, L. Tang, W. Du, X. Feng, B.F. Liu, Microfluidic chip-based C. elegans microinjection system for investigating cell-cell communication in vivo, Biosens. Bioelectron. 50 (2013) 28–34, https://doi.org/10.1016/j.bios.2013.06.024.

[102] A. Noori, P.R. Selvaganapathy, J. Wilson, Microinjection in a microfluidic format using flexible and compliant channels and electroosmotic dosage control, Lab Chip 9 (2009) 3202–3211, https://doi.org/10.1039/B909961A.

[103] W. Wang, X. Liu, D. Gelinas, B. Ciruna, Y. Sun, A fully automated robotic system for microinjection of zebrafish embryos, PLoS One 2 (2007) e862.

[104] D. Koester, A. Cowen, R. Mahadevan, M. Stonefield, B. Hardy, PolyMUMPs Design Handbook, MEMSCAP Inc., 2003.

[105] H.G. Dixit, R. Starr, M.L. Dundon, P.I. Pairs, X. Yang, Y. Zhang, D. Nampe, C.B. Ballas, H. Tsutsui, S.J. Forman, C.E. Brown, M.P. Rao, Massively-Parallelized, deterministic mechanoporation for intracellular delivery, Nano Lett. 20 (2020) 860–867, https://doi.org/10.1021/acs.nanolett.9b03175.

[106] S. Indermun, R. Luttge, Y.E. Choonara, P. Kumar, L.C. Du Toit, G. Modi, V. Pillay, Current advances in the fabrication of microneedles for transdermal delivery, J. Contr. Release 185 (2014) 130–138, https://doi.org/10.1016/j.jconrel.2014.04.052.

[107] P.M. Wang, M. Cornwell, J. Hill, M.R. Prausnitz, Precise microinjection into skin using hollow microneedles, J. Invest. Dermatol. 126 (2006) 1080–1087, https://doi.org/10.1038/sj.jid.5700150.

[108] G. He, J. Feng, A. Zhang, L. Zhou, R. Wen, J. Wu, C. Yang, J. Yang, C. Li, D. Chen, J. Wang, N. Hu, X. Xie, Multifunctional branched nanostraw-electroporation platform for intracellular regulation and monitoring of circulating tumor cells, Nano Lett. 19 (2019) 7201–7209, https://doi.org/10.1021/acs.nanolett.9b02790.

[109] D.W. Bodhale, A. Nisar, N. Afzulpurkar, Structural and microfluidic analysis of hollow side-open polymeric microneedles for transdermal drug delivery applications, Microfluid. Nanofluidics 8 (2010) 373–392, https://doi.org/10.1007/s10404-009-0467-9.

[110] W. Martanto, S.P. Davis, N.R. Holiday, J. Wang, H.S. Gill, M.R. Prausnitz, Transdermal delivery of insulin using microneedles in vivo, Pharm. Res. (N. Y.) 21 (2004) 947–952, https://doi.org/10.1023/B:PHAM.0000029282.44140.2e.

[111] Q.Y. Li, J.N. Zhang, B.Z. Chen, Q.L. Wang, X.D. Guo, A solid polymer microneedle patch pretreatment enhances the permeation of drug molecules into the skin, RSC Adv. 7 (2017) 15408–15415.

[112] A. Vrdoljak, M.G. McGrath, J.B. Carey, S.J. Draper, A.V.S. Hill, C. O'Mahony, A.M. Crean, A.C. Moore, Coated microneedle arrays for transcutaneous delivery of live virus vaccines, J. Contr. Release 159 (2012) 34–42, https://doi.org/10.1016/j.jconrel.2011.12.026.

[113] R.H.E. Chong, E. Gonzalez-Gonzalez, M.F. Lara, T.J. Speaker, C.H. Contag, R.L. Kaspar, S.A. Coulman, R. Hargest, J.C. Birchall, Gene silencing following siRNA delivery to skin via coated steel microneedles: in vitro and in vivo proof-of-concept, J. Contr. Release 166 (2013) 211–219, https://doi.org/10.1016/j.jconrel.2012.12.030.

[114] K.J. Cha, T. Kim, S.J. Park, D.S. Kim, Simple and cost-effective fabrication of solid biodegradable polymer microneedle arrays with adjustable aspect ratio for transdermal drug delivery using acupuncture microneedles, J. Micromech. Microeng. 24 (2014), https://doi.org/10.1088/0960-1317/24/11/115015.

[115] S. Liu, M. Jin, Y. Quan, F. Kamiyama, K. Kusamori, H. Katsumi, T. Sakane, A. Yamamoto, Transdermal delivery of relatively high molecular weight drugs using novel self-dissolving microneedle arrays fabricated from hyaluronic acid and their characteristics and safety after application to the skin, Eur. J. Pharm. Biopharm. 86 (2014) 267–276, https://doi.org/10.1016/j.ejpb.2013.10.001.

[116] L.Y. Chu, M.R. Prausnitz, Separable arrowhead microneedles, J. Contr. Release 149 (2011) 242–249, https://doi.org/10.1016/j.jconrel.2010.10.033.

[117] H. Manoj, P. Gupta, L. Mohan, M. Nagai, S. Wankhar, T.S. Santra, Microneedles: current trends and applications, in: Microfluid. Bio-MEMS, Jenny Stanford Publishing, 2020, pp. 275–342.
[118] S. Zimmermann, D. Fienbork, A.W. Flounders, D. Liepmann, In-device enzyme immobilization: wafer-level fabrication of an integrated glucose sensor, Sensor. Actuator. B Chem. 99 (2004) 163–173, https://doi.org/10.1016/S0925-4005(03)00552-5.
[119] E.V. Mukerjee, S.D. Collins, R.R. Isseroff, R.L. Smith, Microneedle array for transdermal biological fluid extraction and in situ analysis, Sensors Actuators A Phys 114 (2004) 267–275, https://doi.org/10.1016/j.sna.2003.11.008.
[120] K. Kim, J.B. Lee, High aspect ratio tapered hollow metallic microneedle arrays with microfluidic interconnector, Microsyst. Technol. 13 (2007) 231–235, https://doi.org/10.1007/s00542-006-0221-0.
[121] K. Kim, D.S. Park, H.M. Lu, W. Che, K. Kim, J.-B. Lee, C.H. Ahn, A tapered hollow metallic microneedle array using backside exposure of SU-8, J. Micromech. Microeng. 14 (2004) 597–603, https://doi.org/10.1088/0960-1317/14/4/021.
[122] W. Kim, J.K. Ng, M.E. Kunitake, B.R. Conklin, P. Yang, Interfacing silicon nanowires with mammalian cells, J. Am. Chem. Soc. 129 (2007) 7228–7229, https://doi.org/10.1021/ja071456k.
[123] A.K. Shalek, J.T. Gaublomme, L. Wang, N. Yosef, N. Chevrier, M.S. Andersen, J.T. Robinson, N. Pochet, D. Neuberg, R.S. Gertner, I. Amit, J.R. Brown, N. Hacohen, A. Regev, C.J. Wu, H. Park, Nanowire-mediated delivery enables functional interrogation of primary immune cells: application to the analysis of chronic lymphocytic leukemia, Nano Lett. 12 (2012) 6498–6504, https://doi.org/10.1021/nl3042917.
[124] Y.R. Na, S.Y. Kim, J.T. Gaublomme, A.K. Shalek, M. Jorgolli, H. Park, E.G. Yang, Probing enzymatic activity inside living cells using a nanowire-cell "sandwich" assay, Nano Lett. 13 (2013) 153–158, https://doi.org/10.1021/nl3037068.
[125] N. Yosef, A.K. Shalek, J.T. Gaublomme, H. Jin, Y. Lee, A. Awasthi, C. Wu, K. Karwacz, S. Xiao, M. Jorgolli, D. Gennert, R. Satija, A. Shakya, D.Y. Lu, J.J. Trombetta, M.R. Pillai, P.J. Ratcliffe, M.L. Coleman, M. Bix, D. Tantin, H. Park, V.K. Kuchroo, A. Regev, Dynamic regulatory network controlling TH17 cell differentiation, Nature 496 (2013) 461–468, https://doi.org/10.1038/nature11981.
[126] K. Hyungjun, J. Hanmin, K. Bongjoong, K.M. Ku, W.D. Seung, L.H. Soo, K.D. Rip, L.C. Hwan, Flexible elastomer patch with vertical silicon nanoneedles for intracellular and intratissue nanoinjection of biomolecules, Sci. Adv. 4 (2021), eaau6972, https://doi.org/10.1126/sciadv.aau6972.
[127] Y. Chen, S. Aslanoglou, G. Gervinskas, H. Abdelmaksoud, N.H. Voelcker, R. Elnathan, Cellular deformations induced by conical silicon nanowire arrays facilitate gene delivery, Small 15 (2019) 1904819, https://doi.org/10.1002/smll.201904819.
[128] B.G. Nair, K. Hagiwara, M. Ueda, H. Yu, H.-R. Tseng, Y. Ito, High density of aligned nanowire treated with polydopamine for efficient gene silencing by siRNA according to cell membrane perturbation, ACS Appl. Mater. Interfaces 8 (2016) 18693–18700, https://doi.org/10.1021/acsami.6b04913.
[129] C. Chiappini, J.O. Martinez, E. De Rosa, C.S. Almeida, E. Tasciotti, M.M. Stevens, Biodegradable nanoneedles for localized delivery of nanoparticles in vivo: exploring the biointerface, ACS Nano 9 (2015) 5500–5509, https://doi.org/10.1021/acsnano.5b01490.
[130] A.M. Xu, S.A. Kim, D.S. Wang, A. Aalipour, N.A. Melosh, Temporally resolved direct delivery of second messengers into cells using nanostraws, Lab Chip 16 (2016) 2434–2439, https://doi.org/10.1039/C6LC00463F.
[131] S. Park, Y.S. Kim, W.B. Kim, S. Jon, Carbon nanosyringe array as a platform for intracellular delivery, Nano Lett. 9 (2009) 1325–1329, https://doi.org/10.1021/nl802962t.
[132] M. Choi, S.H. Lee, W.B. Kim, V. Gujrati, D. Kim, J. Lee, J. Il Kim, H. Kim, P.E. Saw, S. Jon, Intracellular delivery of bioactive cargos to hard-to-transfect cells using carbon nanosyringe arrays under an applied centrifugal g-force, Adv. Healthc. Mater. 5 (2016) 101–107, https://doi.org/10.1002/adhm.201400834.
[133] G. He, H.J. Chen, D. Liu, Y. Feng, C. Yang, T. Hang, J. Wu, Y. Cao, X. Xie, Fabrication of various structures of nanostraw arrays and their applications in gene delivery, Adv. Mater. Interfac. 5 (2018) 1–8, https://doi.org/10.1002/admi.201701535.
[134] A.M. Xu, A. Aalipour, S. Leal-Ortiz, A.H. Mekhdjian, X. Xie, A.R. Dunn, C.C. Garner, N.A. Melosh, Quantification of nanowire penetration into living cells, Nat. Commun. 5 (2014) 3613, https://doi.org/10.1038/ncomms4613.
[135] A. Aalipour, A.M. Xu, S. Leal-Ortiz, C.C. Garner, N.A. Melosh, Plasma membrane and actin cytoskeleton as synergistic barriers to nanowire cell penetration, Langmuir 30 (2014) 12362–12367, https://doi.org/10.1021/la502273f.
[136] A.M. Xu, D.S. Wang, P. Shieh, Y. Cao, N.A. Melosh, Direct intracellular delivery of cell-impermeable probes of protein glycosylation by using nanostraws, Chembiochem 18 (2017) 623–628, https://doi.org/10.1002/cbic.201600689.
[137] L. Schmiderer, A. Subramaniam, K. Žemaitis, A. Bäckström, D. Yudovich, S. Soboleva, R. Galeev, C.N. Prinz, J. Larsson, M. Hjort, Efficient and nontoxic biomolecule delivery to primary human hematopoietic stem cells using nanostraws, Proc. Natl. Acad. Sci. Unit. States Am. 117 (2020) 21267–21273, https://doi.org/10.1073/pnas.2001367117.
[138] Y. Cao, M. Hjort, H. Chen, F. Birey, S.A. Leal-Ortiz, C.M. Han, J.G. Santiago, S.P. Paşca, J.C. Wu, N.A. Melosh, Nondestructive nanostraw intracellular sampling for longitudinal cell monitoring, Proc. Natl. Acad. Sci. Unit. States Am. 114 (2017) E1866–E1874, https://doi.org/10.1073/pnas.1615375114.
[139] C.B. Fox, Y. Cao, C.L. Nemeth, H.D. Chirra, R.W. Chevalier, A.M. Xu, N.A. Melosh, T.A. Desai, Fabrication of sealed nanostraw microdevices for oral drug delivery, ACS Nano 10 (2016) 5873–5881, https://doi.org/10.1021/acsnano.6b00809.
[140] D. Matsumoto, A. Yamagishi, M. Saito, R.R. Sathuluri, Y.R. Silberberg, F. Iwata, T. Kobayashi, C. Nakamura, Mechanoporation of living cells for delivery of macromolecules using nanoneedle array, J. Biosci. Bioeng. 122 (2016) 748–752, https://doi.org/10.1016/j.jbiosc.2016.05.006.
[141] Z. Zhang, J. Xu, C. Drapaca, Particle squeezing in narrow confinements, 0, Microfluid. Nanofluidics (2018), https://doi.org/10.1007/s10404-018-2129-2, 0.
[142] A.L. McGregor, C.-R. Hsia, J. Lammerding, Squish and squeeze — the nucleus as a physical barrier during migration in confined environments, Curr. Opin. Cell Biol. 40 (2016) 32–40, https://doi.org/10.1016/j.ceb.2016.01.011.
[143] A. Adamo, A. Sharei, L. Adamo, B. Lee, S. Mao, K.F. Jensen, Microfluidics-based assessment of cell deformability, Anal. Chem. 84 (2012) 6438–6443, https://doi.org/10.1021/ac300264v.
[144] A. Sharei, N. Cho, S. Mao, E. Jackson, R. Poceviciute, A. Adamo, J. Zoldan, R. Langer, K.F. Jensen, Cell squeezing as a robust , microfluidic intracellular delivery platform, J. Vis. Exp. 1–7 (2013), https://doi.org/10.3791/50980.
[145] J. Lee, A. Sharei, W.Y. Sim, A. Adamo, R. Langer, K.F. Jensen, M.G. Bawendi, Nonendocytic delivery of functional engineered nanoparticles into the cytoplasm of live cells using a novel, high-throughput microfluidic device, Nano Lett. 12 (2012) 6322–6327, https://doi.org/10.1021/nl303421h.
[146] A. Sharei, R. Trifonova, S. Jhunjhunwala, G.C. Hartoularos, A.T. Eyerman, A. Lytton-Jean, M. Angin, S. Sharma, R. Poceviciute, S. Mao, M. Heimann, S. Liu, T. Talkar, O.F. Khan, M. Addo, U.H. Von Andrian, D.G. Anderson, R. Langer, J. Lieberman, K.F. Jensen, Ex vivo cytosolic delivery of functional macromolecules to immune cells, PLoS One 10 (2015) 1–12, https://doi.org/10.1371/journal.pone.0118803.
[147] G.L. Szeto, D. Van Egeren, H. Worku, A. Sharei, B. Alejandro, C. Park, K. Frew, M. Brefo, S. Mao, M. Heimann, R. Langer, K. Jensen, D.J. Irvine, Microfluidic squeezing for intracellular antigen loading in polyclonal B-cells as cellular vaccines, Sci. Rep. 5 (2015) 10276, https://doi.org/10.1038/srep10276.
[148] T. DiTommaso, J.M. Cole, L. Cassereau, J.A. Buggé, J.L.S. Hanson, D.T. Bridgen, B.D. Stokes, S.M. Loughhead, B.A. Beutel, J.B. Gilbert, K. Nussbaum, A. Sorrentino, J. Toggweiler, T. Schmidt, G. Gyuelveszi, H. Bernstein, A. Sharei, Cell engineering with microfluidic squeezing preserves functionality of primary immune cells in vivo, Proc. Natl. Acad. Sci. Unit. States Am. 115 (2018) E10907–E10914, https://doi.org/10.1073/pnas.1809671115.
[149] A. Sharei, R. Poceviciute, E.L. Jackson, N. Cho, S. Mao, G.C. Hartoularos, D.Y. Jang, S. Jhunjhunwala, A. Eyerman, T. Schoettle, R. Langer, K.F. Jensen, Plasma membrane recovery kinetics of a microfluidic intracellular delivery platform, Integr. Biol. (United Kingdom). 6 (2014) 470–475, https://doi.org/10.1039/c3ib40215k.
[150] M.T. Saung, A. Sharei, V.A. Adalsteinsson, N. Cho, T. Kamath, C. Ruiz, J. Kirkpatrick, N. Patel, M. Mino-kenudson, S.P. Thayer, R. Langer, K.F. Jensen, A.S. Liss, J.C. Love, A size-selective intracellular delivery platform, Small 12 (2016) 5873–5881, https://doi.org/10.1002/smll.201601155.
[151] A. Kollmannsperger, A. Sharei, A. Raulf, M. Heilemann, R. Langer, K.F. Jensen, R. Wieneke, R. Tampé, Live-cell protein labelling with nanometre precision by cell squeezing, Nat. Commun. 7 (2016) 1–7, https://doi.org/10.1038/ncomms10372.
[152] A. Liu, T. Yu, K. Young, N. Stone, S. Hanasoge, T.J. Kirby, V. Varadarajan, N. Colonna, J. Liu, A. Raj, J. Lammerding, A. Alexeev, T. Sulchek, Cell mechanical and physiological behavior in the regime of rapid mechanical compressions that lead to cell volume change, Small 16 (2020) 1–11, https://doi.org/10.1002/smll.201903857.
[153] H. Nejadnik, K.O. Jung, A.J. Theruvath, L. Kiru, A. Liu, W. Wu, T. Sulchek, G. Pratx, H.E. Daldrup-Link, Instant labeling of therapeutic cells for multimodality imaging, Theranostics 10 (2020) 6024–6034, https://doi.org/10.7150/thno.39554.
[154] J. Loo, I. Sicher, A. Goff, O. Kim, N. Clary, A. Alexeev, T. Sulchek, A. Zamarayeva, S. Han, M. Calero-Garcia, Microfluidic transfection of mRNA into human primary lymphocytes and hematopoietic stem and progenitor cells using ultra-fast physical deformations, Sci. Rep. 11 (2021) 1–11, https://doi.org/10.1038/s41598-021-00893-4.
[155] S.-Y. Teh, R. Lin, L.-H. Hung, A.P. Lee, Droplet microfluidics, Lab Chip 8 (2008) 198, https://doi.org/10.1039/b715524g.
[156] P. Prentice, A. Cuschieri, K. Dholakia, M. Prausnitz, P. Campbell, Membrane disruption by optically controlled microbubble cavitation, Nat. Phys. 1 (2005) 107–110, https://doi.org/10.1038/nphys148.
[157] J.M. Meacham, K. Durvasula, F.L. Degertekin, A.G. Fedorov, Enhanced intracellular delivery via coordinated acoustically driven shear mechanoporation and electrophoretic insertion, Sci. Rep. 8 (2018) 1–10, https://doi.org/10.1038/s41598-018-22042-0.
[158] X.-M. Wu, H. Todo, K. Sugibayashi, Enhancement of skin permeation of high molecular compounds by a combination of microneedle pretreatment and iontophoresis, J. Contr. Release 118 (2007) 189–195, https://doi.org/10.1016/j.jconrel.2006.12.017.
[159] H. Chen, H. Zhu, J. Zheng, D. Mou, J. Wan, J. Zhang, T. Shi, Y. Zhao, H. Xu, X. Yang, Iontophoresis-driven penetration of nanovesicles through microneedle-induced skin microchannels for enhancing transdermal delivery of insulin, J. Contr. Release 139 (2009) 63–72, https://doi.org/10.1016/j.jconrel.2009.05.031.
[160] I. Laffafian, M.B. Hallett, Gentle microinjection for myeloid cells using SLAM, Blood 95 (2000) 3270–3271, https://doi.org/10.1182/blood.V95.10.3270.
[161] J. Hurtig, O. Orwar, Injection and transport of bacteria in nanotube–vesicle networks, Soft Matter 4 (2008) 1515, https://doi.org/10.1039/b800333e.
[162] T.H. Wu, Y.C. Wu, E. Sagullo, M.A. Teitell, P.Y. Chiou, Direct nuclear delivery of DNA by photothermal nanoblade, J. Lab. Autom. 20 (2015) 659–662, https://doi.org/10.1177/2211068215583630.

[163] R. Shirakashi, T. Yasui, S. Memmel, V.L. Sukhorukov, Electro-microinjection of fish eggs with an immobile capillary electrode, Biomicrofluidics 9 (2015), https://doi.org/10.1063/1.4936573.
[164] S. Wang, R. Shirakashi, Local Joule heating and electric force on biological membrane during electro-microinjection, Int. J. Heat Mass Tran. 140 (2019) 798–806, https://doi.org/10.1016/j.ijheatmasstransfer.2019.06.010.
[165] K.T. Rodolfa, A. Bruckbauer, D. Zhou, Y.E. Korchev, D. Klenerman, Two-component graded deposition of biomolecules with a double-barreled nanopipette, Angew. Chem. Int. Ed. 44 (2005) 6854–6859, https://doi.org/10.1002/anie.200502338.
[166] C. Rosazza, A. Buntz, T. Rieß, D. Wöll, A. Zumbusch, M.P. Rols, Intracellular tracking of single-plasmid DNA particles after delivery by electroporation, Mol. Ther. 21 (2013) 2217–2226, https://doi.org/10.1038/mt.2013.182.
[167] J. Li, B. Esteban-Fernández de Ávila, W. Gao, L. Zhang, J. Wang, Micro/nanorobots for biomedicine: delivery, surgery, sensing, and detoxification, Sci. Robot. 2 (2017), https://doi.org/10.1126/scirobotics.aam6431 eaam6431.
[168] Z. Yang, L. Deng, Y. Lan, X. Zhang, Z. Gao, C.W. Chu, D. Cai, Z. Ren, Molecular extraction in single live cells by sneaking in and out magnetic nanomaterials, Proc. Natl. Acad. Sci. U.S.A. 111 (2014) 10966–10971, https://doi.org/10.1073/pnas.1411802111.
[169] S.K. Smart, A.I. Cassady, G.Q. Lu, D.J. Martin, The biocompatibility of carbon nanotubes, Carbon N. Y. 44 (2006) 1034–1047, https://doi.org/10.1016/j.carbon.2005.10.011.
[170] I. Laffafian, K.J. Lewis, K.B. Masterman, M.B. Hallett, Microinjection methods for neutrophils, Methods Mol. Biol. 1124 (2014) 181–187, https://doi.org/10.1007/978-1-62703-845-4_11.
[171] Y. Cao, H. Chen, R. Qiu, M. Hanna, E. Ma, M. Hjort, A. Zhang, R.S. Lewis, J.C. Wu, N.A. Melosh, Universal intracellular biomolecule delivery with precise dosage control, Sci. Adv. 4 (2018), https://doi.org/10.1126/sciadv.aat8131.
[172] A. Tay, N. Melosh, Transfection with nanostructure electro-injection is minimally perturbative, Adv. Ther. 2 (2019) 1–9, https://doi.org/10.1002/adtp.201900133.
[173] E. Hebisch, M. Hjort, D. Volpati, C.N. Prinz, Nanostraw-assisted cellular injection of fluorescent nanodiamonds via direct membrane opening, Small 17 (2021) 2006421, https://doi.org/10.1002/smll.202006421.
[174] G. He, C. Yang, T. Hang, D. Liu, H.J. Chen, A.H. Zhang, D. Lin, J. Wu, B.R. Yang, X. Xie, Hollow nanoneedle-electroporation system to extract intracellular protein repetitively and nondestructively, ACS Sens. 3 (2018) 1675–1682, https://doi.org/10.1021/acssensors.8b00367.
[175] R. Wen, A.H. Zhang, D. Liu, J. Feng, J. Yang, D. Xia, J. Wang, C. Li, T. Zhang, N. Hu, T. Hang, G. He, X. Xie, Intracellular delivery and sensing system based on electroplated conductive nanostraw arrays, ACS Appl. Mater. Interfaces (2019), https://doi.org/10.1021/acsami.9b15619.
[176] V. Caprettini, A. Cerea, G. Melle, L. Lovato, R. Capozza, J.A. Huang, F. Tantussi, M. Dipalo, F. De Angelis, Soft electroporation for delivering molecules into tightly adherent mammalian cells through 3D hollow nanoelectrodes, Sci. Rep. 7 (2017) 1–8, https://doi.org/10.1038/s41598-017-08886-y.
[177] J.-A. Huang, V. Caprettini, Y. Zhao, G. Melle, N. Maccaferri, L. Deleye, X. Zambrana-Puyalto, M. Ardini, F. Tantussi, M. Dipalo, F. De Angelis, On-demand intracellular delivery of single particles in single cells by 3D hollow nanoelectrodes, Nano Lett. 19 (2019) 722–731, https://doi.org/10.1021/acs.nanolett.8b03764.
[178] A. Tay, N. Melosh, Mechanical stimulation after centrifuge-free nano-electroporative transfection is efficient and maintains long-term T cell functionalities, Small 17 (2021) 1–11, https://doi.org/10.1002/smll.202103198.
[179] M. Malerba, E. Miele, A. Toma, F. De Angelis, 3D hollow nanostructures for multifunctional plasmonics, in: Conf. Lasers Electro-Optics, Eur. - Tech. Dig., 2014.
[180] M. Dipalo, H. Amin, L. Lovato, F. Moia, V. Caprettini, G.C. Messina, F. Tantussi, L. Berdondini, F. De Angelis, Intracellular and extracellular recording of spontaneous action potentials in mammalian neurons and cardiac cells with 3D plasmonic nanoelectrodes, Nano Lett. 17 (2017) 3932–3939, https://doi.org/10.1021/acs.nanolett.7b01523.
[181] A. Cerea, V. Caprettini, G. Bruno, L. Lovato, G. Melle, F. Tantussi, R. Capozza, F. Moia, M. Dipalo, F. De Angelis, Selective intracellular delivery and intracellular recordings combined in MEA biosensors, Lab Chip 18 (2018) 3492–3500, https://doi.org/10.1039/c8lc00435h.
[182] Z. Wei, S. Zheng, R. Wang, X. Bu, H. Ma, Y. Wu, L. Zhu, Z. Hu, Z. Liang, Z. Li, A flexible microneedle array as low-voltage electroporation electrodes for in vivo DNA and siRNA delivery, Lab Chip 14 (2014) 4093–4102, https://doi.org/10.1039/c4lc00800f.
[183] Y. Zu, S. Huang, Y. Lu, X. Liu, S. Wang, Size specific transfection to mammalian cells by micropillar array electroporation, Sci. Rep. 6 (2016) 1–10, https://doi.org/10.1038/srep38661.
[184] Z. Liu, J. Nie, B. Miao, J. Li, Y. Cui, S. Wang, X. Zhang, G. Zhao, Y. Deng, Y. Wu, Z. Li, L. Li, Z.L. Wang, Self-powered intracellular drug delivery by a biomechanical energy-driven triboelectric nanogenerator, Adv. Mater. 31 (2019) 1–8, https://doi.org/10.1002/adma.201807795.
[185] Z. Liu, L. Li, Self-powered drug-delivery systems based on triboelectric nanogenerator, Adv. Energy Sustain. Res. 2 (2021) 2100013, https://doi.org/10.1002/aesr.202100013.
[186] X. Hou, Y.S. Zhang, G.T. De Santiago, M.M. Alvarez, J. Ribas, S.J. Jonas, P.S. Weiss, A.M. Andrews, J. Aizenberg, A. Khademhosseini, Interplay between materials and microfluidics, Nat. Rev. Mater. 2 (2017), https://doi.org/10.1038/natrevmats.2017.16.
[187] Y. Yu, Q. Wang, C. Wang, L. Shang, Living materials for regenerative medicine, Eng. Regen. 2 (2021) 96–104, https://doi.org/10.1016/j.engreg.2021.08.003.
[188] K. Park, Facing the truth about nanotechnology in drug delivery, ACS Nano 7 (2013) 7442–7447, https://doi.org/10.1021/nn404501g.
[189] Time to deliver, Nat. Biotechnol. 32 (2014) 961, https://doi.org/10.1038/nbt.3045.

Further reading

[94] Y. Zhang, A.C. LeBlanc, Microinjections to study the specific role of proapoptotic proteins in neurons, in: Apoptosis Tech. Protoc., Humana Press, New Jersey, 2002, https://doi.org/10.1385/1-59259-188-4:083, pp. 083–106.